Bull Earthquake Eng (2017) 15:4531–4561
DOI 10.1007/s10518-017-0167-x

ORIGINAL RESEARCH PAPER

Stochastic source, path and site attenuation parameters and associated variabilities for shallow crustal European earthquakes

Sanjay Singh Bora[1] · **Fabrice Cotton**[1,2] · **Frank Scherbaum**[1,2] · **Benjamin Edwards**[3] · **Paola Traversa**[4]

Received: 9 September 2016 / Accepted: 28 May 2017 / Published online: 12 June 2017

Abstract We have analyzed the recently developed pan-European strong motion database, RESORCE-2012: spectral parameters, such as stress drop (stress parameter, $\Delta\sigma$), anelastic attenuation (Q), near surface attenuation (κ_0) and site amplification have been estimated from observed strong motion recordings. The selected dataset exhibits a bilinear distance-dependent Q model with average κ_0 value 0.0308 s. Strong regional variations in inelastic attenuation were also observed: frequency-independent Q_0 of 1462 and 601 were estimated for Turkish and Italian data respectively. Due to the strong coupling between Q and κ_0, the regional variations in Q have strong impact on the estimation of near surface attenuation κ_0. κ_0 was estimated as 0.0457 and 0.0261 s for Turkey and Italy respectively. Furthermore, a detailed analysis of the variability in estimated κ_0 revealed significant within-station variability. The linear site amplification factors were constrained from residual analysis at each station and site-class type. Using the regional Q_0 model and a site-class specific κ_0, seismic moments (M_0) and source corner frequencies f_c were estimated from the site corrected empirical Fourier spectra. $\Delta\sigma$ did not exhibit magnitude dependence. The median $\Delta\sigma$ value was obtained as 5.75 and 5.65 MPa from inverted and database magnitudes respectively. A comparison of response spectra from the stochastic model (derived herein) with that from (regional) ground motion prediction equations (GMPEs) suggests that the presented seismological parameters can be used to represent the corresponding seismological attributes of the regional GMPEs in a host-to-target adjustment framework. The analysis presented herein can be considered as an update of that undertaken for the previous Euro-Mediterranean strong motion database presented by Edwards and Fäh (Geophys J Int 194(2):1190–1202, 2013a).

✉ Sanjay Singh Bora
bora@gfz-potsdam.de

[1] GFZ German Research Center for Geosciences, Potsdam, Germany

[2] University of Potsdam, Potsdam, Germany

[3] Department Earth, Ocean and Ecological Sciences, University of Liverpool, Liverpool, UK

[4] French Electric Company, Aix-en-Provence, France

Keywords Stochastic model · Attenuation · Stress parameter · Kappa · Crustal earthquakes

1 Introduction

Estimation of regional seismological attributes such as source, path and site specific parameters is important in a wide range of applications in seismic hazard analysis. Usually, in engineering seismology and seismic hazard studies strong ground motions (specifically accelerations) are modeled in terms of a stochastic process (Hanks 1979; McGuire and Hanks 1980; Hanks and McGuire 1981) assuming that phases of high frequency waves (ground motions) are random. Typically, the stochastic (amplitude) model is characterized in terms of magnitude and stress parameter ($\Delta\sigma$) as being the source parameters; the geometrical spreading and anelastic attenuation (Q) of seismic wave describe the path effects. The site effects are modeled in terms of crustal amplification (Boore 2003; Joyner et al. 1981; Boore and Joyner 1997) and site-related attenuation parameter (κ_0).

We have analyzed the recently developed pan-European strong motion database, RESORCE-2012 (Akkar et al. 2014a) in order to estimate these spectral parameters. In addition to estimate these seismological parameters that describe the amplitude and shape of Fourier spectra of strong ground motion, we also focus our discussion on variability and trade-off issues. More specifically, we analyze the following key issues related with the stochastic modelling of ground motion:

(1) A European stochastic model has been derived by Edward and Fäh (2013a). This model was based upon a strong-motion database compiled more than a decade ago and, due to limited data, did not include regional variations in attenuation properties within Europe. The analysis of more recent strong-motion database indicates that regional variations of ground motions may be significant (Boore et al. 2014; Kotha et al. 2016; Kuehn and Scherbaum 2016) which is a motivation to evaluate the regional variations of stochastic ground motions parameters in Europe.

(2) One of the major challenges in ground motion prediction is that motions need to be predicted for earthquakes without knowing the (future) stress-parameter ($\Delta\sigma$) associated with them. Therefore, usually blind predictions are made for an average value of $\Delta\sigma$ with an associated standard deviation. Often, the average $\Delta\sigma$ is assumed to be independent of magnitude (Aki 1967), however recent studies have indicated, that for small to moderate earthquakes ($M_W < 5$) $\Delta\sigma$ may increase with increasing magnitude and the average $\Delta\sigma$ can also vary regionally (Malagnini et al. 2008; Edwards et al. 2008; Drouet et al. 2008, 2010; Yenier and Atkinson 2015a, b). Other than the magnitude dependence and regional variation, the spread (standard deviation) in estimated $\Delta\sigma$ is also important in predicting ground motions for future scenarios (Cotton et al. 2013).

(3) The decay of high frequency Fourier spectral amplitudes beyond the Brune's corner frequency f_c is usually attributed to (an empirical parameter) κ (kappa) (Anderson and Hough 1984) that essentially captures the combined effect of whole path anelastic attenuation (Q) and near site attenuation κ_0. Extrapolation of κ at near distances (≈ 0) is termed as κ_0 and is believed to reflect near site attenuation. In a site-specific seismic hazard application, knowing κ_0 beforehand at a target site is of crucial importance. As shown by Molkenthin et al. (2014) and Douglas and Jousset

(2011) in a stochastic simulation framework, pseudo spectral accelerations (PSA) for small to moderate events at high oscillator frequencies >10 Hz are mainly controlled by κ_0. However, measurement of a true site κ_0 is not straightforward because the observed traces are recorded at a non-zero distance, which makes decoupling of path term (Q) and κ_0 rather challenging without constraining any of the two a priori. In this context, regional variation of Q, as will be shown in this article, can also bias the estimation of κ_0. Thus, the trade-off between Q and κ_0 needs to be analyzed and accounted in the forward prediction as well.

(4) Several studies have shown that κ_0 varies significantly from site-to-site and regionally as well (e.g., Atkinson and Morrison 2009; Edwards et al. 2008; Campbell 2009; Edwards and Rietbrock 2009). The site-to-site/station-to-station variability of κ_0 will be referred as between-station variability. The other component of variability in κ_0 is related to the record-to-record (or within-station) variability. Within-station variability of κ_0 can also have a strong impact on the site-to-site adjustment of GMPEs in the HTTA framework. However, this within-station variability has not been discussed much in past studies.

Assuming ω^2 point-source model (Brune 1970, 1971)—which has been shown to be applicable to $M_W < 6$ events globally, and a reasonable approximation for larger events at high frequencies (Chen and Atkinson 2002; Baltay and Hanks 2014)—a broadband (generalized) inversion technique (Edwards and Fäh 2013a; Bora et al. 2015) is performed to determine the source, path and site parameters.

Essentially, the inversion method remains the same as detailed in Bora et al. (2015) in which a full Fourier amplitude spectrum is used to estimate Brune's source corner frequency (f_c) and the whole path inelastic attenuation operator (t^*) simultaneously. The inverted t^* values are further analyzed to derive a frequency-independent Q_0 model for the dataset and to analyze regional variation in Q_0 within the selected dataset. The choice of a particular Q_0 model is seen to have a large impact on the derived κ_0 values. With respect to the regional Q_0 models, we investigated two different components of variability in station κ_0 in terms of station-to station variability (between-station) and record-to-record variability (within-station). After constraining the reference model by using the database M_0 and regional inelastic attenuation Q_0 models, average residuals are used to capture the linear part of the site amplification in the Fourier domain (Edwards et al. 2013; Drouet et al. 2010; Poggi et al. 2011). The final estimation of source f_c and M_0 is obtained from site-effects corrected spectra, which are further analyzed to estimate stress parameter ($\Delta\sigma$) values.

2 Data

Different subsets of the RESORCE-2012 database have been used to derive several pan-European GMPEs (Akkar et al. 2014b; Bindi et al. 2014; Bora et al. 2014; Derras et al. 2014; Hermkes et al. 2014). The same dataset as used by Bora et al. (2015) is used in this study. This dataset is a subset of a larger parent database of RESORCE-2012 (Akkar et al. 2014a) and it contains strong motion recordings made across Europe, the Mediterranean region and the Middle East. To ensure the validity of the point-source (Brune model) approximation, we have discarded near distance traces from large magnitude earthquakes (Bora et al. 2015). For events with moment magnitude $M_W < 5.5$ no trace was discarded; for events with $5.5 \leq M_W < 6.5$ traces recorded at hypocentral distance $R < 15$ km were

Fig. 1 Metadata summary of the selected dataset. **a** Distribution of earthquake epicenters. **b** M_W-hypocentral distance distribution. **c** M_W-depth distribution. **d** *Light-shade* high-pass and *dark-shade* low-pass frequency. **e** Number of records per station versus number of stations

discarded; and for $M_W \geq 6.5$, traces recorded at $R < 30$ km were not considered. The dataset consists of 1200 (2400 including both the horizontal components) acceleration traces recorded at 350 stations from 365 earthquakes. Figure 1 summarizes the main metadata features of the selected dataset. Figure 1a depicts geographical distribution of epicenters from the selected dataset. The magnitude and distance range covered by the present dataset is M_W 4–7.6 and hypocentral distance up to 224 km respectively (Fig. 1b). The station Vs_{30} values range from 92 to 2165 m/s out of which 223 are measured and rest are inferred from different methods. All the events are shallow crustal events up to the focal depth of 30 km (Fig. 1c). For complete metadata information of the recordings, the reader is referred to the electronic supplement supplied with Bora et al. (2015). The processed database was disseminated to ensure a uniform data processing scheme for empirical ground motion prediction equation (GMPE) derivation.

Additionally, for our analysis we use the Fourier amplitudes only between the useable frequency limits. We chose the filter high-pass and low-pass frequencies as the useable frequency limits, if a record is not assigned a low-pass frequency in the metadata then a flat low-pass frequency of 50 Hz was chosen. It is worth mentioning here that no smoothing is applied over the observed Fourier spectral amplitudes prior to the inversion except that the amplification curves are presented after smoothing (Konno and Ohmachi 1998) observed Fourier amplitude spectra. Figure 1d shows the distribution of high-pass and low-pass frequencies in the dataset, while Fig. 1e depicts the number of records per station against the number of stations.

3 Fourier spectral inversion

We use the Brune (1970, 1971) point source model with a single corner frequency (f_c) to characterize the far field Fourier spectrum of acceleration records. In the stochastic modelling framework (Boore 1983, 2003), assuming that the high frequency ground motions of engineering interests are randomly distribution in phase the Fourier spectral amplitude Y at a frequency, f can be modeled using the following analytical relationship (Bora et al. 2015):

$$Y(f) = CM_0G(R)\left\{\frac{(2\pi f)^2}{1+\left(\frac{f}{f_c}\right)^2}\right\}e^{-\pi f t^*}A(f). \quad (1)$$

In Eq. (1), M_0 is the seismic moment in units of Nm and f_c is the corner frequency in Hertz, given by $0.4906\beta(\Delta\sigma/M_0)^{1/3}$ (Eshelby 1957; Brune 1970, 1971), in which $\Delta\sigma$ is the stress parameter in Mega Pascal and β (=3500 m/s) is the shear wave velocity in the vicinity of the source. The constant C is generally taken as $\Theta_{\lambda\varphi}F\xi/\left(4\pi\rho\beta^3\right)$, in which $\Theta_{\lambda\varphi}$ (=0.55) is the average radiation pattern for S waves (Boore and Boatwright 1984), F (=2.0) is the near surface amplification, $\xi\left(=1/\sqrt{2}\right)$ is a factor to account for the partition of total shear-wave energy into two horizontal components, and ρ (=2800 kg/m^3) is the average density near the source (Boore 1983, 2003). $G(R)$ is the geometrical spreading function

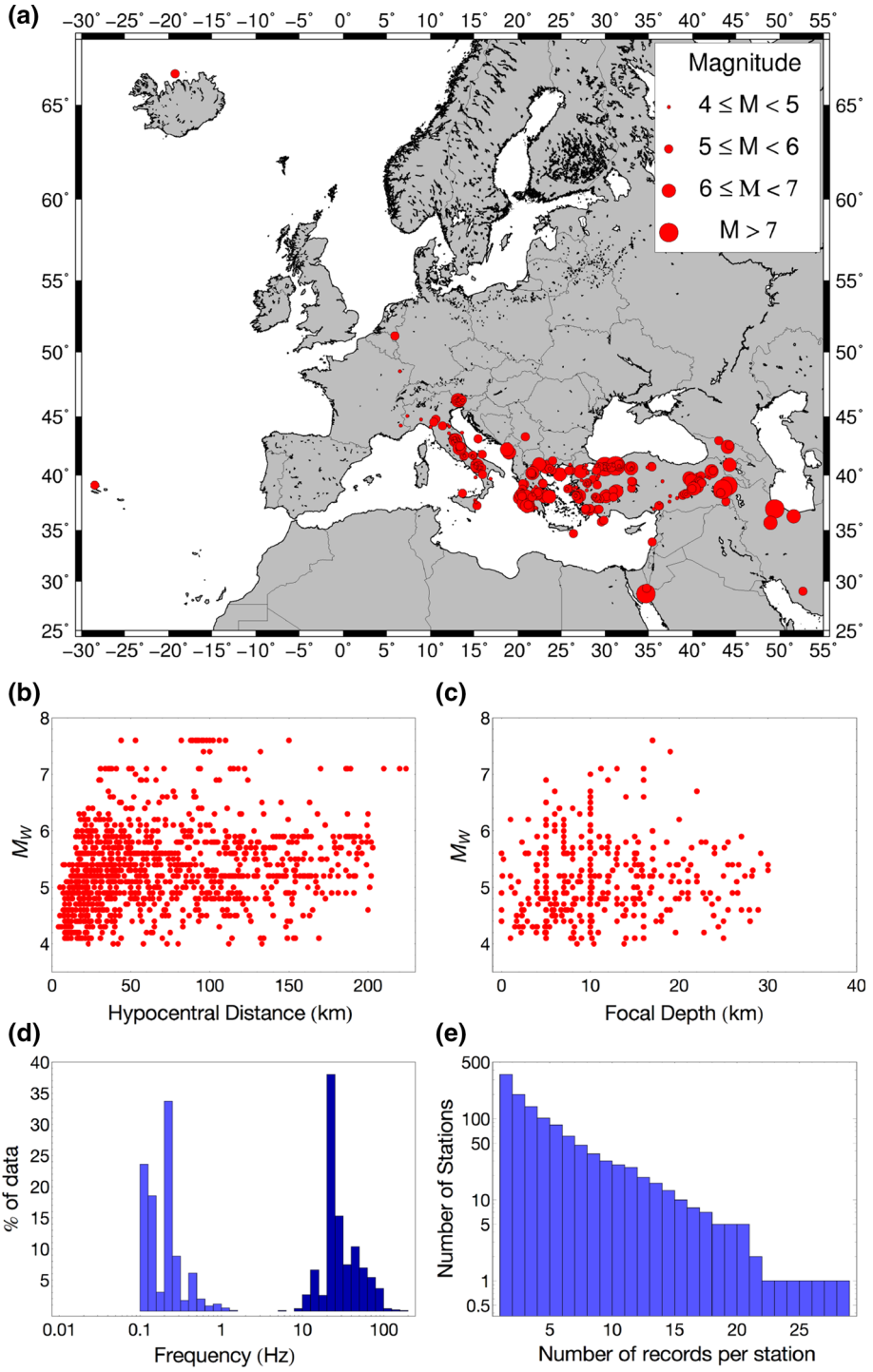
(a)
Magnitude
4 ≤ M < 5
5 ≤ M < 6
6 ≤ M < 7
M > 7
(b)
M_W
Hypocentral Distance (km)
(c)
M_W
Focal Depth (km)
(d)
% of data
Frequency (Hz)
(e)
Number of Stations
Number of records per station

representing a frequency-independent decay of amplitude as function of distance. Theoretically, $G(R)$ is equal to $1/R$ at near distances ($<\sim 50$ to 100 km) for an isotropic and homogenous whole space. However, the earth is not homogeneous and many studies have found it to be a complex function of distance (Campillo et al. 1984; Atkinson and Mereu 1992; Edwards et al. 2008; Atkinson and Boore 2011). To limit potential trade-off and bias, $G(R)$ is constrained by using an earlier derived $G(R)$ model from the same dataset in Bora et al. (2015) as:

$$G(R) = \begin{cases} \left(\frac{R_0}{R}\right)^{1.14} & R \leq 70 \\ \left(\frac{R_0}{R_1}\right)^{1.14} \left(\frac{R_1}{R}\right)^{0.5} & R > 70 \end{cases} \quad (2)$$

In Eq. (2), R_0 is assumed to be 1 km. Bora et al. (2015) derived the $G(R)$ model from low-frequency (0.2–1 Hz) Fourier spectral amplitudes to minimize the trade-off resulting from high-frequency attenuation Q.

The fall-off of acceleration spectra at high frequencies is modeled by using a whole-path anelastic attenuation operator (t^*). t^* is alternatively named $\kappa(R)$ (Anderson and Hough 1984) and κ_r (Ktenidou et al. 2014). The t^* implies spectral decay at high frequencies due to path and site effects, while some authors (e.g., Kilb et al. 2012) argue contribution of source effects in t^* as well. The combined effect of anelastic attenuation Q and site-related attenuation κ_0 (Ktenidou et al. 2014) in t^* is represented by the following equation:

$$t^* = \frac{R}{Q\beta} + \kappa_0 \quad (3)$$

in which β (= 3.5 km/s) is the average shear wave velocity used to infer Q and R is the hypocentral distance. Some studies have suggested (Singh et al. 1982; Atkinson and Mereu 1992; Malagnini et al. 2000; Bay et al. 2003; Atkinson 2004; Drouet et al. 2008; Malagnini et al. 2011; Akinci et al. 2014) a Q model as a function of frequency as follows:

$$Q(f) = Q_0 \left(\frac{f}{f_0}\right)^{\eta} \quad (4)$$

in which, η ranges from 0, for a frequency-independent Q, to 1 and Q_0 is the reference Q value at $f_0 = 1$ Hz. However, estimation of Q from spectra of observed recordings is strongly tied with the assumed geometrical spreading (e.g. Pacor et al. 2016). As shown by Edwards et al. (2008) a frequency-dependent Q function can lead to a strong trade-off with the geometrical spreading. Furthermore, Morozov (2008, 2009) have suggested that from a modeling perspective distinction between frequency-dependent Q and geometric attenuation is ambiguous. Thus, some studies (Anderson and Hough 1984; Hough et al. 1988; Edwards et al. 2008, 2011; Campbell 2009; Edwards and Fäh 2013a) in engineering seismology also use a frequency-independent $Q = Q_0$ (constant) over the frequency-band it is measured. Thus in this article, we restrict our model formulation to a constant-Q model. It is beyond the scope of this article to investigate sensitivity of a chosen Q model (frequency-independent or constant) over the parameters derived here, however a constant-Q is expected to give lower κ_0 value than that with a frequency-dependent Q. Nevertheless, the derived parameter values (with a constant-Q assumption) are consistent within the entire model framework (taking geometrical spreading, $\Delta\sigma$, Q_0 and κ_0 together). $A(f)$ in

Eq. (1) represents site amplification, which essentially captures the effect of impedance contrast during the wave propagation from the half-space through the upper soil layers to the station.

In our inversion scheme the observed spectra are inverted with respect to the natural log of the model described in Eq. (1) to determine M_0, f_c and t^* using a least squares fit in which the Newton's method is used to linearize the nonlinear equation. To address the problem of two unresolved degrees of freedom, that is, M_0 and $A(f)$, in the first iteration of inversion the low-frequency spectral level is constrained by using M_0 obtained from the database M_W (Hanks and Kanamori 1979). Thus, database M_0 values and f_c and t^* determined from the first iteration of inversion, essentially describe our reference model. This reference model along with a generic crustal amplification function defines the motion at the base of the soil column beneath the station. The (logarithmic) difference between the observed amplitude and the amplitude obtained by the combination (addition in log) of reference model and the generic crustal amplification is used to constrain the amplification $A(f)$ at a given station (for details see section Site Amplification). The final estimates of f_c and M_0 are obtained from site-corrected, $A(f)$, spectra.

The inversion was performed over the full spectrum between the high-pass and low-pass frequencies of each record given in the metadata file. If a record is not assigned with a low-pass frequency then a flat low-pass frequency limit of 50 Hz is used. It is also known that site-effects can potentially bias the determination of seismological parameters from the surface recorded spectra. From records recorded at rock and hard rock site stations, determination of t^* can be biased due to significant resonance effects at high frequencies (Parolai and Bindi 2004; Edwards et al. 2015). Similarly, at soft soil sites, resonance effects present at low frequencies can bias the determination of f_c. However, in the present dataset majority of the earthquakes are of small to moderate magnitudes (M_W 4–5.5), hence we believe that the corresponding f_c values will remain unaffected from the resonance effects. Furthermore, an event-wise (common for all records originated from an event) determination of f_c can limit the potential bias due to the site-effects (Edwards et al. 2008). In order to limit bias in the determination of t^* due to crustal amplification, we correct all the spectra for a reference rock amplification function (Bora et al. 2015; Edwards et al. 2015). Also, fitting the entire shape (determined by f_c and t^*) of the spectrum simultaneously limits the error in t^* estimation that may arise due to the resonance peaks at high frequencies. The majority of the stations in the selected dataset are located over soil or stiff-soil sites ($180 < Vs_{30} \leq 750$ m/s). The generic rock amplification of California (Boore and Joyner 1997) anchored at Vs_{30} 620 m/s was considered to be appropriate as reference rock amplification for the present dataset.

4 Attenuation parameters: t^*, Q_0 and κ_0

As mentioned in the previous section, in the first step of our broadband inversion scheme we determine f_c and t^* simultaneously based upon the model described in Eq. (1) while seismic moments are constrained from database M_W values (Akkar et al. 2014a) using the relationship of Hanks and Kanamori (1979). In our analysis, we use hypocentral distance as the preferred distance metric, following Edwards and Fäh (2013a). We obtain two t^* values per record, one for each component, however in order to limit the scatter in data points, a mean t^* (from both the components) is used here. Performing a least-squares linear fit using Eq. (3), over the dataset that contains t^* values against R (hypocentral

distance), we find dataset common Q_0 (dividing the slope by β) and κ_0 (the intercept) values as 1029 and 0.0361 s respectively. The 68% confidence interval of the best-fit slope corresponds to Q_0 values 982 and 1080. Similarly, the 68% confidence interval of the intercept gives κ_0 values of 0.035 and 0.0372 s.

In terms of comparison between Q_0 values form this study and those from earlier studies, Edwards and Fäh (2013a) obtained the Q_0 value as 619 from broadband fit using a smaller subset of the present dataset. In their study, Edwards and Fäh (2013a) used records only up to 100 km of hypocentral distance. Edwards et al. (2011) and Douglas et al. (2010) presented Q_0 values 1216 and 1630 for Switzerland and France respectively using the records up to 300 km; while in this study we use records up to 224 km. Thus, this difference in Q_0 values can be due to the differences arising from data-selection criteria, distance metric used and the actual regional difference in Q_0. The choice of distance range in fitting $t^* - R$ data can also influence the estimated Q_0 values.

In order to further explore the distance dependent estimation of Q_0, we plot median of sorted (by distance) $t^* - R$ data in each 10 km distance bin, and as can be observed from Fig. 2a a clear trend indicating distance-dependent attenuation, Q_0, (varying slope of $t^* - R$ relationship) is visible. As a cross-check, we also analyzed the t^* values obtained from high-frequency linear fit method (Anderson and Hough 1984). The lower limit of the high-frequency range was selected (automatically) such that it is sufficiently above than the source f_c for each record for an assumed $\Delta\sigma$ of 10 MPa and database M_W. The upper limit of the frequency range was either fixed to the low-pass frequency given in the metadata information or to 50 Hz for the records that are not assigned a low-pass frequency. Finally, only those t^* values were selected which were measured over a band of at least 10 Hz. The high frequency fit t^* values are plotted against distance in Fig. 2b and a binning scheme similar to the one in Fig. 2a was applied on the $t^* - R$ data. A similar trend to that in Fig. 2a can also be observed in Fig. 2b indicating that the $t^* - R$ relationship from the selected dataset shows a distance-dependent slope (hence Q_0). This observation was validated further from least square fit on the actual $t^* - R$ data (without binning and averaging them) assuming a bilinear relationship with a slope-transition distance of 40 km. It can also be observed from Fig. 2a, b that, the straight-line fit of $t^* - R$ data gives different zero-distance intercept, κ_0, whereas the values are rather identical for a bilinear fit. Hence a single linear fit model of $t^* - R$ relationship might overestimate the κ_0 values. Anderson (1991) has also suggested that if a straight line fit does not fit the data well, any other

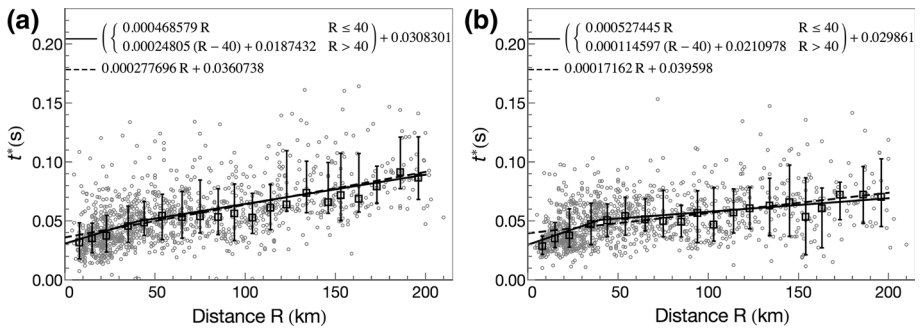

Fig. 2 t^*-distance relationship from the entire dataset. **a** From broadband inversion method. **b** From high-frequency linear fit method (Anderson and Hough 1984). The *empty circles* indicate the individual data points while the *empty squares* indicate the median of $t^* - R$ data in each 10 km distance bin. The extent of *vertical bars* indicate the t^* values corresponding to 16 and 84 percentiles in each distance bin

smooth functional form can be chosen. Selection of a bilinear form for $t^* - R$ relationship against more complicated (e.g., quadratic R) forms was based upon a compromise between simplicity and effectiveness of the model in capturing the observed trend. Assuming an average $\beta = 3.5$ km/s, the Q_0 values at $R \leq 40$ and $R > 40$ km were obtained as: 610 and 1152 from broadband fit t^* and 542 and 2493 from high-frequency fit t^* values.

In order to investigate the regional variations in inelastic attenuation we split the $t^* - R$ data in three regional categories based upon the station locations: (1) stations located in Turkey, (2) stations located in Italy and (3) the remaining stations in the dataset. Although the physical properties are not expected to follow the political boundaries, our criterion for selecting data in different nation-regions is rather simple and based upon a similar criterion used in recent NGA-West2 GMPEs, e.g., Abrahamson et al. (2014) and Boore et al. (2014). The $t^* - R$ data for the three region categories is plotted in Fig. 3. As can be noted from Fig. 3, the majority of the data belongs to Turkey with 667 data points, followed by 372 from Italy and the remaining 161. Out of the three, only data from Turkey shows a uniform distribution with distance, the data from Italy and remaining stations is mostly concentrated at <70–80 km. Similar to Fig. 2, the $t^* - R$ data is binned in 10 km distance bins and corresponding median values and spread in each bin is also plotted over the actual distribution of the data. Although, one may observe a distance dependent variation in slope, a straight line fit over $t^* - R$ data from Turkey captures the observed trend reasonably well. The Italian data is mostly concentrated at smaller distances. Nevertheless, the straight line fit captures the observed trend well over the full distance range. Due to the very limited data points beyond 80 km, the fit was performed only up to 80 km for the remaining $t^* - R$ data (Fig. 3c). It is worth mentioning that, the fitted lines shown in Fig. 3 are obtained from the fitting of actual data points. Using $\beta = 3.5$ km, the Q_0 values and associated variabilities for the three region categories are shown in Fig. 4a. Figures 3 and 4a clearly indicate that within the selected dataset and at large in the RESORCE database, there are strong regional variations in anelastic attenuation. The data from Turkey exhibits rather low attenuation (high Q_0) in comparison to that for Italy, an observation that was also noted by Boore et al. (2014) and Kotha et al. (2016) in their empirical models.

Estimation of κ_0 using Eq. (3) is strongly biased upon the assumed Q model. Consequently, and as can also be observed in Fig. 4b, a higher Q_0 gives a higher κ_0 and similarly lower κ_0 is obtained for a lower Q_0. A smaller variability in Q_0 and κ_0 (Fig. 4b) for Italy in comparison to that for Turkey can be attributed to that the Italian dataset is mainly concentrated at smaller distances. Hence, the ray paths are mostly sampling similar (shallower) depths in the subsurface, thus fewer variations due to anelastic attenuation. For

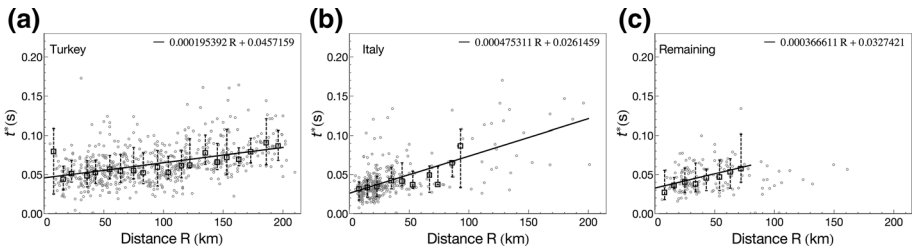

Fig. 3 t^*-distance model for: **a** Turkey, **b** Italy, **c** and remaining dataset. *Empty circles* indicate individual data points while *empty squares* represent the median of $t^* - R$ data in each 10 km distance bin, while the extent of *vertical bars* indicates the t^* values corresponding to 16 and 84 percentiles in the bins

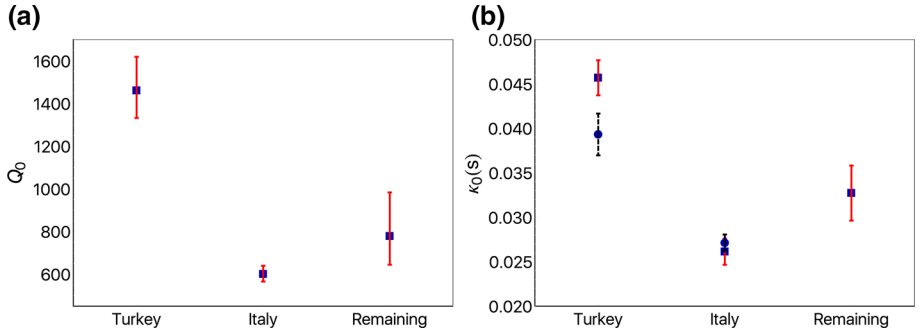

Fig. 4 Regional variations in inelastic attenuation parameter $\boldsymbol{Q_0}$ (**a**) and site-related attenuation $\boldsymbol{\kappa_0}$ (**b**). The *squares* in (**b**) indicate average $\boldsymbol{\kappa_0}$ values when the respective $\boldsymbol{Q_0}$ values of (**a**) are used while the *discs* indicate the $\boldsymbol{\kappa_0}$ values when the database based bilinear $\boldsymbol{Q_0}$ model shown in Fig. 2a is used. The extent of the *vertical bars* corresponds to the 68% confidence interval of each parameter estimate

the remaining dataset, the large uncertainty can be explained due to its regional heterogeneity. Therefore, depth variations in Q_0 can be expected as well as the regional variations. In order to further investigate the regional variations in κ_0, we constrained Q_0 from the common (database) bilinear model shown in Fig. 2a to estimate the average κ_0 in Turkey and Italy. Additionally, we limit the data only up to 50 km for this analysis to constrain the bias from Q_0 variations. As expected due to the coupling of Q_0 and κ_0, one can observe in Fig. 4b that the κ_0 values are different than that when we use regional Q_0 values (Fig. 4a) for Turkey and Italy. However, the rather important observation is that using a common Q_0 value for the two regional datasets also indicates a significant variation in attenuation properties for Turkey and Italy due to surficial layers as near distance earthquakes are expected to sample near-surface structure of the subsurface. Hereafter, regional Q_0 values for Turkey and Italy will be used for further analysis. While for the remaining dataset the database based distance-dependent Q_0 model (Fig. 2a) will be used.

5 Station and site-class specific κ_0

In stochastic simulations (Boore 2003) as well as in HTTA adjustments of empirical GMPEs a prior measurement of κ_0 at a given site is required (e.g., Campbell 2003; Van Houtte et al. 2011; Edwards et al. 2016). In order to obtain a station-specific κ_0 estimate, we correct all the individual record t^* (both the components individually) for the slope in $t^* - R$ straight-line fit corresponding to regional Q_0 values, that is, 1462 for Turkey and 601 for Italy. For the remaining dataset, the database based, the two-slope $t^* - R$ model presented in Fig. 2a is used. Subsequently, the median of all record κ_0 values at a station is presented as the station κ_0. Table 1 presents estimated κ_0 values for 45 stations recording at least 14 component-records.

Figure 5 depicts variation of station κ_0, and associated variability with Vs_{30} for stations with $Vs_{30} > 360$ m/s and with minimum ten records (including both the components). Figure 5a depicts the plot only for stations that have recorded earthquakes located at a distance $\leq$40 km. As mentioned earlier, regional variation in Q models can bias the estimation of κ_0; thus Turkish stations are observed to exhibit consistently higher κ_0. An important observation from Fig. 5 is that, there is a rather large record-to-record (within-

Table 1 Station specific κ_0 estimation for stations recording at least seven records

Station Id	Station Country	Vs_{30} (m/s)	N	κ_0 (s)		
				50 Percentile	16 Percentile	84 Percentile
3	Italy	1029.6	14	0.022	0.016	0.032
19	Italy	162.1	14	0.027	0.018	0.039
129	Italy	444.7	14	0.027	0.018	0.03
148	Turkey	283.3	14	0.03	0.022	0.039
184	Turkey	316	14	0.029	0.026	0.038
187	Turkey	481.3	14	0.021	0.017	0.025
190	Turkey	616.4	14	0.037	0.031	0.049
3633	Italy	679.2	14	0.031	0.019	0.037
10	Italy	600	16	0.029	0.028	0.037
146	Turkey	282	16	0.027	0.022	0.08
162	Turkey	338.6	16	0.02	0.008	0.032
188	Turkey	293.6	16	0.063	0.02	0.081
2462	Turkey	354.8	16	0.04	0.034	0.059
2635	Turkey	228.7	16	0.032	0.03	0.049
3612	Italy	835.5	16	0.022	0.02	0.03
124	Italy	219.3	18	0.029	0.023	0.037
136	Turkey	285.5	18	0.045	0.032	0.111
147	Turkey	408.7	18	0.039	0.033	0.049
169	Turkey	338.6	18	0.03	0.019	0.037
105	Turkey	355.9	20	0.038	0.03	0.068
3620	Italy	199	20	0.044	0.006	0.055
183	Turkey	455.7	21	0.032	0.026	0.043
120	Italy	142.6	22	0.03	0.019	0.043
231	Turkey	407.3	22	0.046	0.035	0.072
2503	Turkey	480.8	22	0.041	0.032	0.048
2987	Italy	684.8	22	0.013	0.008	0.032
3679	Italy	488	22	0.01	0.004	0.026
2465	Turkey	267.4	24	0.041	0.036	0.051
3614	Italy	473.7	24	0.014	0.009	0.036
138	Turkey	242.5	26	0.066	0.047	0.083
140	Turkey	456.6	26	0.051	0.043	0.059
2322	Turkey	746.9	26	0.05	0.04	0.071
2459	Turkey	366.9	27	0.038	0.033	0.044
229	Turkey	528.7	28	0.042	0.033	0.052
2591	Turkey	374.9	28	0.062	0.054	0.065
2466	Turkey	232.9	30	0.04	0.022	0.053
2984	Italy	716.5	30	0.019	0.009	0.033
122	Italy	554.8	32	0.021	0.014	0.026
149	Turkey	595.2	34	0.03	0.024	0.048
153	Turkey	191.8	34	0.046	0.034	0.067
8	Italy	454.4	40	0.021	0.018	0.031
139	Turkey	662	40	0.048	0.04	0.064

Table 1 continued

Station Id	Station Country	Vs_{30} (m/s)	N	κ_0 (s)		
				50 Percentile	16 Percentile	84 Percentile
155	Turkey	412	40	0.03	0.023	0.041
131	Italy	534	42	0.012	0.008	0.02
134	Turkey	270	56	0.059	0.045	0.074

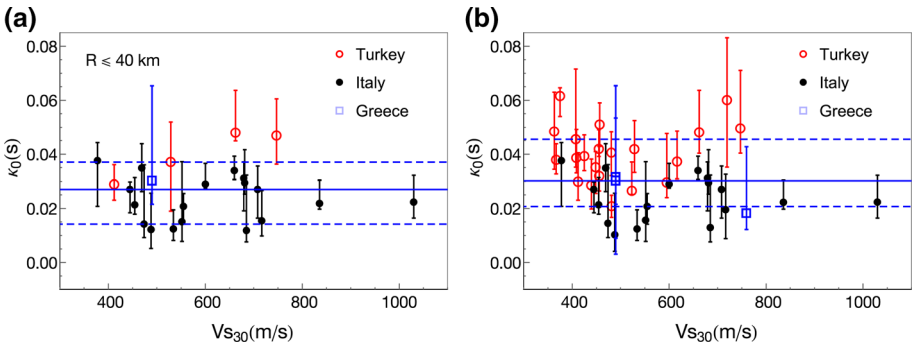

Fig. 5 Station κ_0 plotted against Vs_{30} values for $Vs_{30} > 360$ m/s: **a** when earthquakes located at <40 km (from a station) are used, **b** when all the earthquakes recorded at a station are used. Markers (*empty circles*, *disks* and *empty squares*) indicate the median while the extent of *vertical bars* indicates the values corresponding to 16 and 84 percentiles at each station, i.e., within-station variability. The *horizontal solid line* indicates the median value of all station κ_0 in the sample, while two *dashed lines* indicate 16 and 84 percentile values in the sample, i.e. between-station variability. In both cases stations which have recorded at least 10 records (including both the components) are used

station) variability (the vertical bars) in κ_0, which in many cases is comparable to the station-to-station (between-station) variability (horizontal dashed-lines) of κ_0. The between-station variability is mainly affected by regional variations in Q_0. Although we did not observe a clear correlation between κ_0 and Vs_{30} (Fig. 5b), the between-station variability can also increase since softer sites may exhibit higher κ_0 (Chandler et al. 2006; Van Houtte et al. 2011; Edwards and Fäh 2013a). On the other hand, the within-station variability is due to the fact that Q_0 is not homogeneous with respect to depth (Edwards et al. 2008; Edwards et al. 2011). Hence estimating κ_0 from near as well as distant earthquakes using a homogenous Q model can also inflate the within-station variability. As can also be noted from Fig. 5b: the Italian stations depict less within-station variability in comparison to the Turkish stations. Additionally, a possible source component in κ_0 (Kilb et al. 2012) can also contribute to the larger within-station variability. Figure 6 demonstrates the effect of within-station variability in κ_0 by showing plots of spectra obtained from actual fit and that from regional Q_0 and station κ_0, vis-à-vis observed spectra. The spectra are shown at a station in Turkey with $Vs_{30} = 747$ m/s and for earthquakes at less than 40 km distance from the station.

In order to cover a broad range of station sites, we also estimate site class specific κ_0 values, which can be used as a first order approximation for stations not having endemic measurements of κ_0. In addition to the regional classification based upon Q_0, stations were classified in different site-classes based upon their Vs_{30} values as: very soft soil as

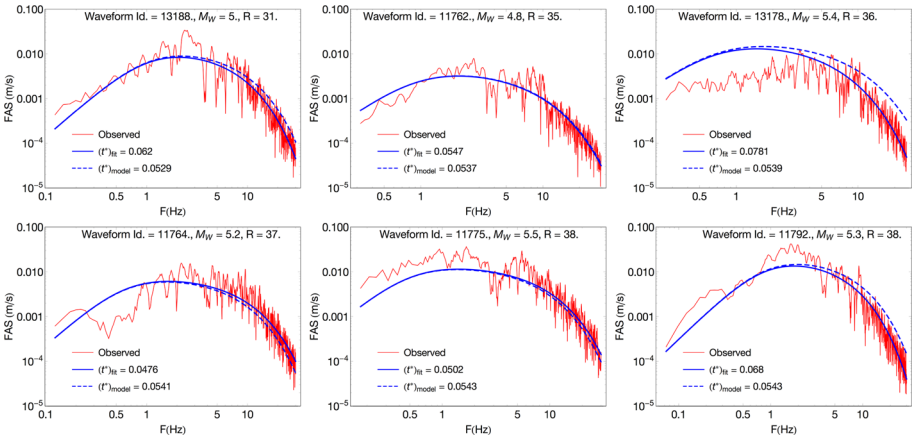

Fig. 6 Within station variability of $\boldsymbol{\kappa_0}$. Spectra for acceleration traces recorded at a station (Stn. Id. 2322) in Turkey with a $\boldsymbol{Vs_{30}}$ of 747 m/s. The regional $\boldsymbol{Q_0}$ 1462 for Turkey is used along with the station $\boldsymbol{\kappa_0}$ 0.0468 s

$Vs_{30} \leq 180$ m/s, $180 < Vs_{30} \leq 360$ m/s as soft soil, $360 < Vs_{30} \leq 750$ m/s as stiff soil and $Vs_{30} > 750$ m/s as rock sites. Subsequently the site class κ_0, in each regional subset, is computed as the median of all record κ_0. The site class specific κ_0 and corresponding variabilities are presented in Table 2. A rather large κ_0 for rock sites in Turkey can be a sampling issue with only eight data points. For Italian sites we observe a decreasing κ_0 from very soft soil sites to rock sites. In the remaining dataset, there were no stations corresponding to the very soft soil site condition. For a combined (data from all regions), but significantly limited subset of this dataset, Edwards and Fäh (2013a) obtained κ_0 as 0.0326, 0.0375, 0.0303 and 0.0241 s for very soft soil, soft soil and stiff soil and rock site respectively. The values of site class κ_0 for Turkish dataset from this study are comparable with the findings of Askan et al. (2014) with κ_0 values 0.0377 and 0.0455 s in stiff and soft soil category.

6 Station and site-specific amplification

We invert for a reference model using a priori seismic moments and geometrical spreading from Bora et al. (2015). The station (Fourier) site amplification factors (AF_{Fourier}) are estimated with respect to this reference model from a residuals analysis (Edwards et al. 2008; Drouet et al. 2010; Edwards and Fäh 2013a). For the reference model, M_0 is used from database M_W and t^* values were fixed to a value that is obtained from a combination of regional Q_0 and station κ_0 derived in the previous section. In order to obtain the site AF_{Fourier} at one station, we take mean of all (log) residuals (at each frequency) with respect to the reference model. Out of total 350, only 223 stations characterized with measured Vs_{30} estimates are used in the site amplification analysis.

Figure 7 depicts AF_{Fourier} plots for selected stations, which have recorded at least ten horizontal records (five earthquakes), except for a station (station Id. 2498) in Greece. Stations with station Ids 131 and 3690 indicate resonance effects present at such sites, which are consistent with the notion that stiff soil/rock sites may indicate resonance peaks at high frequencies while at softer soil sites such effects are mostly dominant at lower frequencies. It is worth to note here that, for determining AF_{Fourier}, we additionally

Table 2 Site-class specific estimates of κ_0 in each regional subset

Site class	κ_0 (s)											
	Turkey				Italy				Remaining			
	N	16 Per	50 Per	84 Per	N	16 Per	50 Per	84 Per	N	16 Per	50 Per	84 Per
Very soft soil	14	0.0273	0.0395	0.0472	32	0.0185	0.029	0.0618	0	–	–	–
Soft soil	330	0.0265	0.0433	0.0675	83	0.0172	0.0271	0.0436	43	0.011	0.0267	0.0469
Stiff soil	315	0.0275	0.0416	0.0605	219	0.0099	0.0224	0.0387	96	0.0122	0.0271	0.0429
Rock	8	0.0317	0.0495	0.0662	38	0.0076	0.0212	0.0322	22	0.0048	0.0232	0.0447

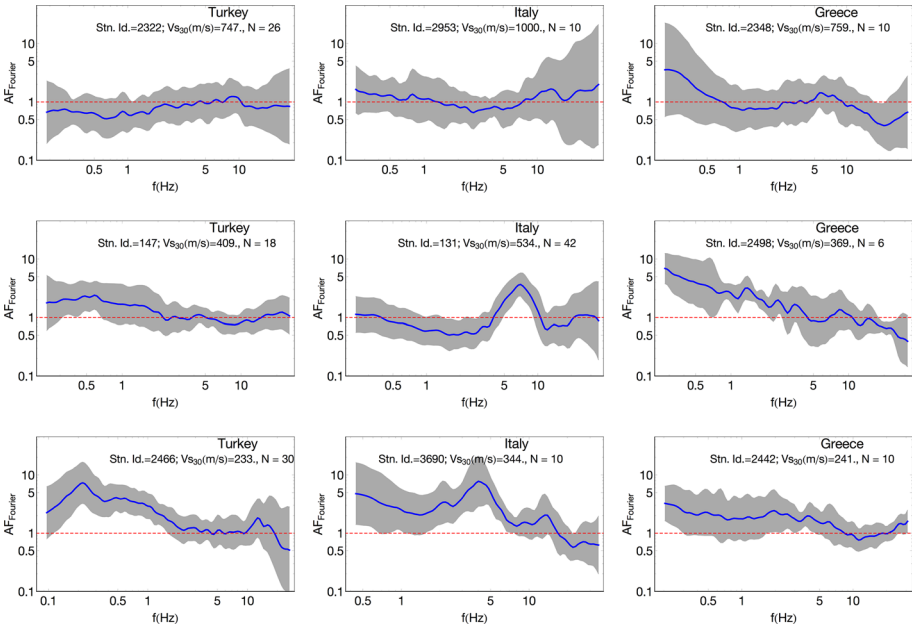

Fig. 7 Station-specific Fourier amplification curves for selected stations. The *thick curve* indicates mean amplification and the *gray shaded bands* indicate extent of the standard deviation. It may be noted that the site amplification curves are presented only for the stations, which are characterized by a measured $\boldsymbol{Vs_{30}}$ estimate

excluded the records recorded at $R \leq 60$ km (from earthquakes with $M_W \geq 6.5$) to avoid the nonlinear soil response effects. Consistent with our site-class specific κ_0 estimates, we also present site-class specific amplification factors AF_{Fourier} for the four site classes for each regional subset in Fig. 8. Such plots also provide guidance in defining the amplification at stations for which direct measurements of *Vs*-profiles are not available. Although, resonance peaks are not apparent in the site-class AF_{Fourier} curves due to the broad site classification, the very soft and soft soil site indicate a large amplification at lower frequencies, and a deamplification at large frequencies may indicate (residual) non-linear site effects. Whereas, the stiff soil and rock sites indicate amplifications almost independent of frequency. Regional variations in site-class average site amplification factors are not apparent from Fig. 8. Rock motions show an amplification close to one, which indicates that the reference is well calibrated. Also, the overall slight-deamplification for rock ($Vs_{30} > 750$ m/s) in Turkey is consistent with respect to the chosen reference amplification of California (Boore and Joyner 1997) anchored at Vs_{30} 620 m/s. However, the similar AF_{Fourier} curves for stiff soil and rock conditions in Italy indicate towards misclassification for some of the stations (Lucia Luzi, *personal communication*). It is worth emphasizing again that these amplification curves are obtained with respect to a crustal reference amplification of Boore and Joyner (1997) by removing it from the observed spectra. Therefore, Boore and Joyner (1997) crustal amplification curve should be used along with these AF_{Fourier} curves in a forward prediction application.

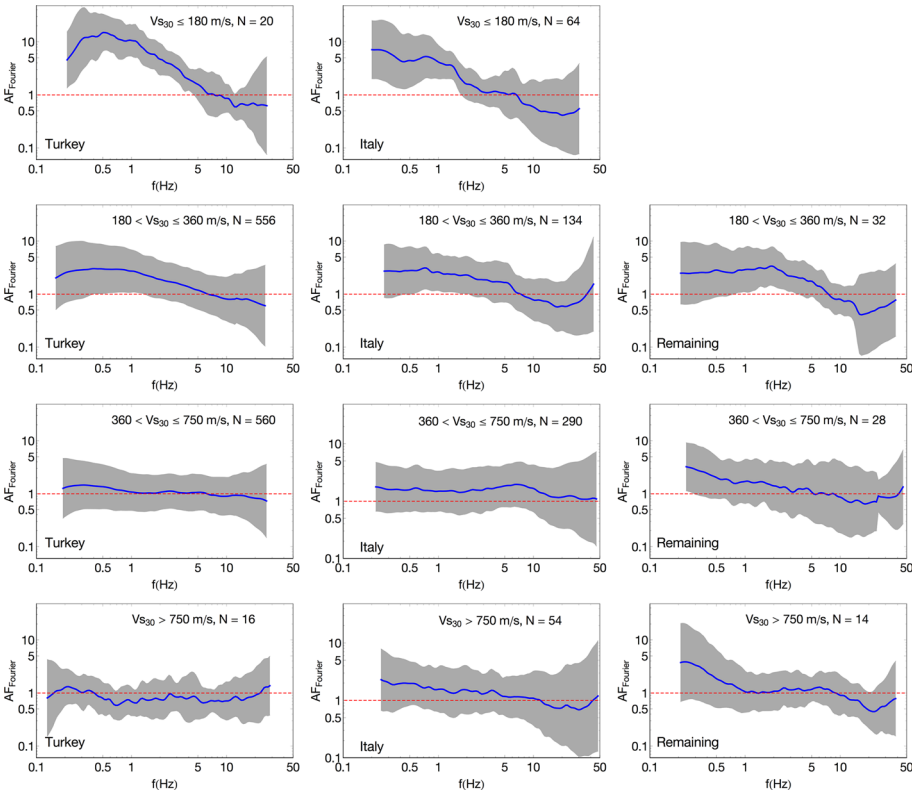

Fig. 8 Region-wise site class-specific Fourier amplification. The *thick curve* indicates the mean amplification and the *gray shaded bands* indicate the extent of one standard deviation

7 Source parameters M_W and $\Delta\sigma$

After estimating the site amplification curves, AF_{Fourier}, we refit the site-corrected spectra to determine event-specific f_c as well as seismic moments. We use site-class specific AF_{Fourier} curves (Fig. 8) to correct the observed spectra for site amplification effects. The site-class AF_{Fourier} curves represents the site amplification effects over a broad range of stations; hence obviously they may not capture the detailed amplification characteristics of a single station, rather reflecting a typical feature. Nevertheless, they allow including the stations, which have recorded fewer earthquakes and also limiting the bias due to those fewer recordings.

In this iteration, other than the geometrical spreading function, the high frequency slope t^* is fixed to the value that is a combination of regional Q_0 models and a regional site-class κ_0 (Table 2). The fitting is focused to fit the low frequency spectral level of the acceleration spectrum, i.e., $f \leq 10$ Hz. In order to avoid the trade-off between M_W (magnitude) and $\Delta\sigma$ at frequencies beyond f_c, we do not include the high frequency spectral amplitudes in fitting at this stage. The choice of 10 Hz is rather subjective and is based on the assumption that this can be the highest f_c in the dataset as most of the earthquakes are of low-to-moderate magnitudes ($M \geq 4$). In Brune's (1970, 1971) source model for far-field

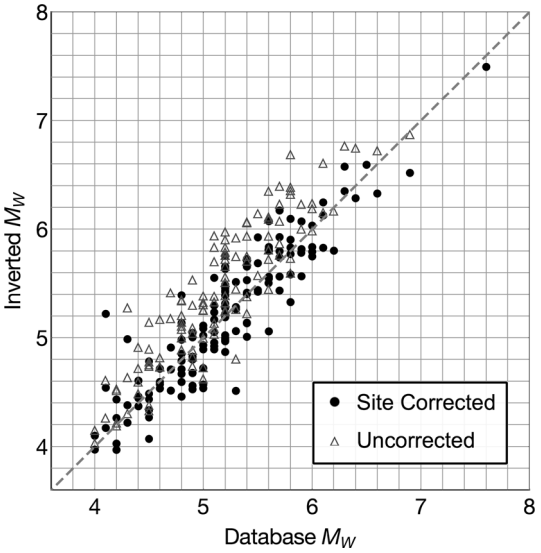

Fig. 9 Comparison of inverted M_W with that from database. *Disks* when inverted M_W are obtained from site-class specific amplification corrected; and *empty triangles* when inverted M_W are obtained from uncorrected spectra. Events that have been recorded at least at three stations (six records including both the components) are shown

spectrum of displacement motion, the spectral amplitude Y (plateau) below f_c is related to M_0 as:

$$Y(f \ll f_c) = \frac{M_0 \xi \theta F}{4\pi\beta^3 \rho}. \tag{5}$$

In Eq. (5), the values, of near source density (ρ), near source average shear wave velocity (β), average radiation coefficient for S_H waves (θ), energy partition coefficient (ξ) and free surface amplification factor (F) remain the same as used in Eq. (1). The estimated M_0 is used to compute the inverted magnitude M_W using the Hanks and Kanamori (1979) relation. Almost 1:1 correlation can be observed between database and inverted M_W in Fig. 9. However, the over prediction of M_W values from uncorrected spectra illustrates the challenge in estimating M_W values from observed Fourier spectra in presence of significant site-effects.

The inverted f_c and M_W are used to compute the stress parameters ($\Delta\sigma$) using the following relationship:

$$\Delta\sigma = M_0 \left(\frac{f_c}{0.4906\beta} \right) \tag{6}$$

(Brune 1970, 1971; Eshelby 1957) where β is the near-source shear wave velocity assumed to be 3500 m/s. Figure 10a depicts the variation of $\Delta\sigma$ values with respect to database M_W and Fig. 10b illustrates the same variation with focal depth. To obtain a robust estimate of inverted f_c and M_W, events recorded on at least three stations are used for this analysis. As found for the previous database (Edwards and Fäh 2013a) Fig. 10a does not show any magnitude dependency of $\Delta\sigma$. Thus, assuming a constant $\Delta\sigma$ model, the $\Delta\sigma$ (in MPa) using inverted M_W is obtained as:

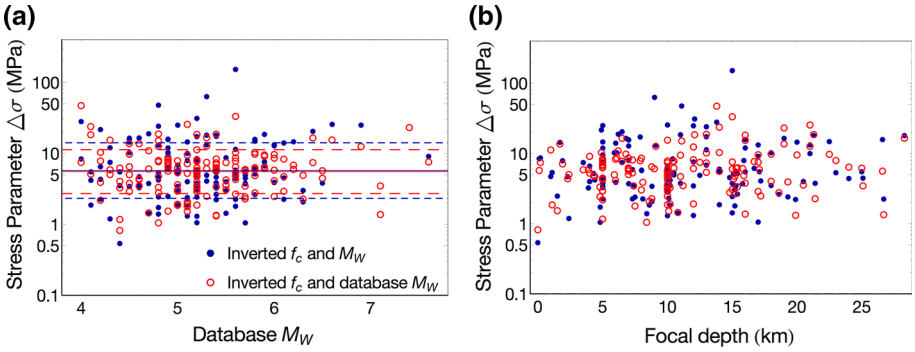

Fig. 10 Stress parameters ($\boldsymbol{\Delta\sigma}$) (obtained from site-class specific amplification corrected spectra) plotted against database $\boldsymbol{M_W}$ in panel (**a**) against depth in panel (**b**). *Disks* indicate the $\boldsymbol{\Delta\sigma}$ values when both $\boldsymbol{f_c}$ and $\boldsymbol{M_W}$ were obtained from inversion while the *empty circles* indicate those when only $\boldsymbol{f_c}$ was obtained from inversion keeping the $\boldsymbol{M_0}$ fixed from database $\boldsymbol{M_W}$. Again, events recorded at least at three stations (six records including both the components) are shown

$$\log_{10}\Delta\sigma = \log_{10} 5.75 \pm 0.43. \tag{7}$$

If we constrain M_0 to a value from database M_W and invert for f_c only, the median $\Delta\sigma$ is obtained identical to that in Eq. (7) with smaller (lognormal) standard deviation as:

$$\log_{10}\Delta\sigma = \log_{10} 5.65 \pm 0.33 \tag{8}$$

The median $\Delta\sigma$ values are slightly smaller than those obtained by Edwards and Fäh (2013a) as 8.8 and 7.4 MPa from inverted and database M_W respectively, while the standard deviations are comparable. The $\Delta\sigma$ variability obtained in this study is also comparable with that inferred (Cotton et al. 2013) from between-event variability in the GMPEs of Akkar et al. (2014a), Boore et al. (2014) and Bindi et al. (2014) as: 0.43, 0.42 and 0.41 respectively.

Additionally, we estimated $\Delta\sigma$ for the M_W 4.8 St. Die earthquake, as it has been widely investigated and discussed in the literature (e.g., Scherbaum et al. 2004). Although, the station-specific Vs_{30} values are not available for the stations recording St. Die earthquake, the soil type information of those stations was obtained from RESIF seismic data portal (http://seismology.resif.fr/). Out of the nine stations, three stations were classified in the EC (Eurocode)-8 soil type E, two in soil type B and the remaining four were classified in soil type A. We did not apply any corrections to empirical Fourier spectra to account for the local site amplification effects except correcting for the crustal amplification related with the generic rock amplification of California (Boore and Joyner 1997). However, the t^* values were fixed using the two separate κ (or t^*) models (i.e., for soil and rock) of Douglas et al. (2010), as some of the stations (which recorded St. Die earthquake) are included in their analysis as well. Fixing the low frequency spectral level by the M_0 obtained from database M_W gives the $\Delta\sigma$ value as 49.2 MPa, while inverting for both f_c and (M_0) magnitude gives $\Delta\sigma$ as 32.3 MPa corresponding to the fitted M_W 4.96. Such high values are consistent with high ground motion amplitudes observed for this event.

The values of $\Delta\sigma$ determined in this study are compared in the context of recent studies involving $\Delta\sigma$ determination for mainland Europe (Edwards and Fäh 2013a, b) in Fig. 11. Edwards and Fäh (2013a) involves earthquakes from all over Europe and the Mediterranean, which is essentially a subset of the present dataset, while the analysis of Edwards

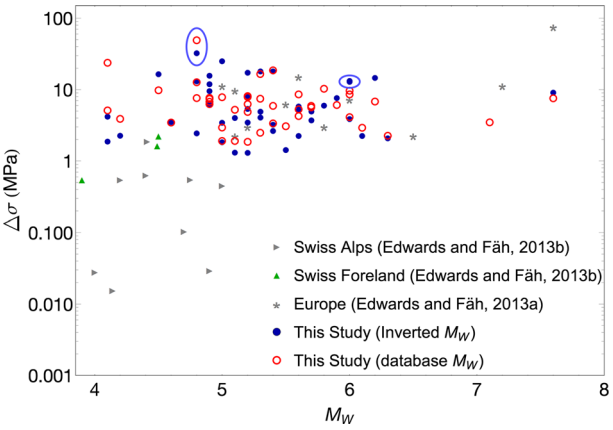

Fig. 11 **Δσ** comparison with the previous studies from the same region. Events recorded at least at seven stations (fourteen records including both the components) are shown in this figure. The *encircled* markers indicate the Δσ values (*left* and *right*) corresponding to St. Die and Friuli earthquakes respectively

and Fäh (2013b) is based upon the earthquake from Swiss Alps and Swiss Foreland basin. Δσ values from present study are observed to be in good comparison to the other studies except that the earthquakes from Swiss Alps are exhibiting lower Δσ values.

Apart from St. Die earthquake, that is exhibiting a relatively larger Δσ, we did not observe discernable regional pattern in Δσ (from the present dataset) as suggested by some recent studies (Malagnini et al. 2008; Drouet et al. 2010; Yenier and Atkinson 2015b; Goertz-Allmann and Edwards 2014). The Friuli earthquake M_W 6, 1976 also indicates a large Δσ of 13.38 MPa with inverted M_W 5.79, while using the database M_W gives Δσ as 8.6 MPa. In Fig. 11, earthquakes recorded at least at seven stations (fourteen records including both the components) are shown. For the earthquakes shown in Fig. 11, inverted f_c, M_W, Δσ and the associated uncertainties are given in Table 3.

8 Discussion

From the present analysis, we observed regional variations in anelastic attenuation Q_0 and κ_0 from shallow active crustal earthquakes recorded across Europe and Mediterranean. Although, estimation of κ_0 is strongly linked with how one constrains Q_0, our analysis also indicates that it may also vary significantly between Turkey and Italy. As some studies have investigated correlation of κ_0 with deeper structure (Campbell 2009; Ktenidou et al. 2015), there is a possibility that κ_0 has regional component (Ktenidou et al. 2015), which depends on varying crustal properties.

Furthermore, within a single region, significant, record-to-record (within-station) variability in κ_0 is observed, which in many cases is comparable to the station-to-station (between-station) variability. Large within-station variability can be expected when a station records earthquakes over a range of distances. Thus the waves reaching at the station may encounter different anelastic attenuation regimes due to sampling deeper layers as well as the shallower layers in the subsurface. Essentially this variability is entering in κ_0 through the depth variation of Q_0. For the estimation of κ_0 therefore it is recommended to use records from near station earthquakes in addition to account for regional differences

Table 3 Stress parameter values for earthquakes recorded on at least seven stations

Eq. id	Eq. country	Eq. name	Y	M	D	H	M	S	Depth h (km)	N	Inverted M_W							Database M_W				
											M_W	M_{WMin}	M_{WMax}	f_c	$\Delta\sigma$	$\Delta\sigma$ M_{WMin}	$\Delta\sigma$ M_{WMax}	M_W	f_c	$\Delta\sigma$	$\Delta\sigma$ M_{WMin}	$\Delta\sigma$ M_{WMax}
57	Italy	Friuli	1976	09	15	09	21	18	7	16	5.77	5.74	5.8	0.51	13.38	11.5	15.57	6	0.34	8.6	8.41	8.8
96	Italy	NA	1981	01	16	00	37	45	10.5	14	5.33	5.3	5.36	0.56	3.9	3.3	4.6	5.2	0.71	5.06	4.93	5.2
531	Italy	Umbria	1997	09	26	00	33	12	7	18	5.94	5.91	5.98	0.26	3.37	2.83	4.02	5.7	0.41	5.27	5.18	5.36
533	Italy	Umbria	1997	09	26	09	40	25	6	18	6.05	6.02	6.08	0.24	3.52	2.93	4.21	6	0.26	3.85	3.79	3.91
543	Italy	App.	1997	10	06	23	24	53	3.9	16	5.75	5.71	5.78	0.31	2.77	2.29	3.35	5.4	0.57	5.3	5.2	5.4
551	Italy	Umbria	1997	10	14	15	23	09	7.3	14	6.11	6.07	6.15	0.18	1.92	1.57	2.33	5.6	0.44	4.78	4.72	4.84
927	Turkey	Kocaeli	1999	08	17	00	01	39	17	33	7.53	7.5	7.56	0.06	9.12	7.77	10.71	7.6	0.05	8.11	8.06	8.16
970	Turkey	Izmit	1999	08	19	15	17	45	12	16	5.36	5.35	5.38	0.36	1.17	1.08	1.28	5.1	0.58	1.95	1.93	1.97
982	Turkey	Izmit	1999	08	22	14	31	00	14	14	5.27	5.25	5.29	0.47	1.81	1.64	2.01	4.1	4.32	25.29	24.32	26.28
1056	Turkey	Izmit	1999	08	31	08	10	49	4	30	5.25	5.24	5.26	0.63	4.24	4	4.5	5.1	0.84	5.81	5.75	5.87
1115	Greece	Ano	1999	09	07	11	56	51	17	18	5.77	5.75	5.78	0.59	20.19	18.35	22.21	6	0.39	12.78	12.58	12.99
1146	Turkey	Izmit	1999	-09	13	11	55	30	14	54	6.12	6.11	6.14	0.26	6.19	5.7	6.72	5.8	0.47	11.23	11.14	11.31
1172	Turkey	Izmit	1999	09	20	21	28	00	15	24	5.43	5.41	5.44	0.43	2.44	2.21	2.69	4.8	1.32	8.1	7.98	8.22
1203	Turkey	Izmit	1999	09	29	00	13	06	12	14	5.7	5.67	5.73	0.35	3.32	2.84	3.88	5.2	0.85	8.47	8.32	8.62
1245	Turkey	Izmit	1999	11	07	16	54	41	7	22	4.59	4.58	4.6	2.02	14.13	13.32	14.97	4.9	1.08	6.3	6.19	6.42
1256	Turkey	Izmit	1999	11	11	14	41	23	8	46	5.85	5.84	5.86	0.35	5.76	5.36	6.2	5.6	0.55	9.23	9.15	9.3
1427	Turkey	Duzce	1999	11	13	00	54	54	5	14	4.6	4.58	4.61	2.37	23.14	21.24	25.17	5	1.04	7.97	7.75	8.21
1484	Turkey	Duzce	1999	11	16	17	51	17	5	16	5.01	4.99	5.03	0.74	2.9	2.62	3.22	5	0.75	2.95	2.9	3.01
1501	Turkey	Duzce	1999	11	19	19	59	06	5	20	4.72	4.71	4.73	1.6	10.76	9.97	11.61	4.9	1.11	6.83	6.68	6.98
2065	Turkey	Duzce	2000	08	23	13	41	28	15	14	5.97	5.93	6.01	0.19	1.4	1.15	1.71	5.5	0.44	3.27	3.23	3.32
2454	Turkey	Demirtas	2001	06	22	11	54	50	10	16	5.44	5.42	5.45	0.34	1.27	1.17	1.38	5.2	0.52	1.99	1.97	2.01
2814	Turkey	Seferihisar	2003	04	10	00	40	14	10	14	5.84	5.82	5.86	0.34	4.8	4.38	5.26	5.7	0.43	6.21	6.14	6.28
2959	Turkey	NA	2003	06	09	17	44	03	9.1	16	4.82	4.82	4.83	1.49	12.58	11.98	13.22	4.8	1.56	13.37	13.17	13.57
3004	Turkey	NA	2003	07	23	04	56	05	28.3	14	5.31	5.29	5.32	0.95	17.55	16.33	18.85	5.3	0.96	17.78	17.47	18.1
3037	Turkey	NA	2003	07	26	01	00	57	5	14	4.84	4.83	4.85	1.32	9.24	8.65	9.87	4.9	1.17	8.01	7.86	8.16

Table 3 continued

Eq. id	Eq. country	Eq. name	Y	M	D	H	M	S	Depth h (km)	N	Inverted M_W							Database M_W				
											M_W	M_{WMin}	M_{WMax}	f_c	$\Delta\sigma$	$\Delta\sigma$ M_{WMin}	$\Delta\sigma$ M_{WMax}	M_W	f_c	$\Delta\sigma$	$\Delta\sigma$ M_{WMin}	$\Delta\sigma$ M_{WMax}
3054	Turkey	NA	2003	07	26	08	36	10	21.3	14	5.46	5.45	5.47	0.8	17.69	16.52	18.93	5.4	0.9	20.13	19.82	20.45
3405	Turkey	NA	2004	12	20	23	02	15	12.5	16	5.56	5.54	5.57	0.46	4.74	4.36	5.15	5.3	0.73	7.84	7.74	7.95
3553	Turkey	NA	2006	02	08	04	07	42	6.8	14	4.35	4.35	4.36	2.83	17.24	16.33	18.18	4.5	2.06	10.96	10.75	11.17
3641	Turkey	NA	2006	10	20	18	15	26	16.7	36	5.03	5.03	5.04	0.91	6.03	5.83	6.24	4.9	1.17	8.02	7.96	8.09
3650	Turkey	NA	2006	10	24	14	00	22	7.9	52	4.9	4.9	4.9	1.51	17.02	16.64	17.41	5.2	0.84	8.44	8.38	8.49
3774	Turkey	NA	2007	11	09	01	43	05	15.9	16	5.01	5	5.01	1.02	7.7	7.37	8.04	5.2	0.71	5.06	5.01	5.12
3932	Montenegro	Montenegro	1979	05	24	17	23	18	5	14	5.74	5.73	5.76	0.63	22.88	20.74	25.22	6.2	0.28	9.39	9.21	9.58
4699	Italy	L	2009	04	06	01	32	39	8.8	14	6.33	6.3	6.37	0.14	2.11	1.8	2.49	6.3	0.15	2.25	2.22	2.27
4703	Italy	L	2009	04	07	09	26	28	10.2	14	5.01	5	5.02	0.62	1.75	1.64	1.87	5	0.63	1.79	1.77	1.82
4704	Italy	L	2009	04	07	17	47	37	15.1	28	5.5	5.49	5.51	0.49	4.76	4.52	5.02	5.6	0.41	3.96	3.93	4
4705	Italy	Aquila	2009	04	07	21	34	29	7.4	16	4.59	4.58	4.6	1.22	3.07	2.9	3.24	4.6	1.19	2.98	2.94	3.03
4706	Italy	Aquila	2009	04	08	22	56	50	10.2	14	4.16	4.15	4.17	2.08	3.48	3.32	3.66	4.1	2.36	4.12	4.04	4.19
4707	Italy	Gran	2009	04	09	00	52	59	15.4	26	5.54	5.53	5.56	0.37	2.35	2.19	2.52	5.4	0.48	3.06	3.03	3.09
4709	Italy	Aquila	2009	04	09	04	32	44	8.1	14	4.43	4.42	4.44	1.22	1.79	1.69	1.89	4.2	1.91	3.08	3.03	3.14
4710	Italy	Aquila	2009	04	09	19	38	16	17.2	18	5.07	5.06	5.08	0.74	3.55	3.37	3.75	5.3	0.48	2.21	2.19	2.24
4747	Turkey	Kovancilar	2010	03	08	02	32	39	5	14	6.3	6.27	6.32	0.15	2.11	1.84	2.42	6.1	0.21	3.01	2.98	3.04
4749	Turkey	Simav	2011	05	19	20	15	23	12	86	5.82	5.81	5.83	0.4	7.61	7.35	7.88	5.9	0.35	6.52	6.49	6.56
4993	France	St. Die	2003	02	22	20	41		5	18	4.955	4.94	4.96	1.75	32.3	30.88	33.78	4.8	2.41	49.2	48.42	49.98

Min and Max correspond to the 68% confidence limit in fitted M_W and f_c

in Q_0. Large within-station variability in κ_0 can also be contributed by the source-component present in κ_0 (Kilb et al. 2012). From an application perspective, for example in stochastic simulations and HTTA adjustment of GMPEs, a linked (or combined) Q and κ_0 model should be used to maintain the consistency. Finally, an important consequence of larger within-station variability (in κ_0) from the GMPE adjustment perspective is that it can hinder the effect of site (station) corrections made in κ_0 to account for site-to-site variability. This article presents broad site-class based κ_0 measurements for the regional subsets as well as the station-specific κ_0. We did not observe a clear relationship between κ_0 and Vs_{30} as suggested by some other studies.

8.1 Comparison with previous studies

A meaningful comparison between the estimated parameters with previous studies can only be possible when underlying assumptions (e.g., mainly geometrical spreading) and method of estimation is the same amongst the studies. Nevertheless, anelastic attenuation Q, $\Delta\sigma$ and κ_0 for different regions across Europe and Mediterranean from some representative studies are given in Table 4 along with the assumed geometrical spreading function. To facilitate comparison with a frequency-independent Q_0 from our study, we have fixed Q at 10 Hz from the studies involving frequency dependent Q. As expected a significant variation amongst the studies can be seen in Table 4. The Q_0 values determined in this study agree with the general trend that Turkey and Greece exhibit higher Q values (lower attenuation) in comparison to that in Italy. Our Q_0 estimates for Turkey are consistent with the findings for the northwestern part (Kurtulmus and Akyol 2013; Askan et al. 2014), which is expected as the majority of our Turkish records come from this region. Similarly, the κ_0 value for Turkey from our study is in good agreement with the value of 0.045 s found by Akinci et al. (2013) for Anatolian region in Turkey. Moreover, recent GMPEs (Boore et al. 2014; Kotha et al. 2016; Kuehn and Scherbaum 2016) have also indicated regionally varying anelastic attenuation terms indicating a higher Q in Turkey and lower Q in Italy. The present dataset does not permit to investigate regional variations in $\Delta\sigma$. The average median $\Delta\sigma$ value of 5.65 MPa from our analysis for the entire region is broadly consistent with the previous studies, except with the very high values of 20 and 60 MPa from Umbria-Marche and northeastern regions in Italy (Malagnini and Herrmann 2000; Malagnini et al. 2000). However, as stated earlier, comparisons amongst the parameter estimates should be made relative to the geometrical spreading function rather than treating them as absolute values.

8.2 Stochastic model predictions

We validate the model parameters derived in this study by comparing the model predictions against recorded data. The comparison is performed in terms of graphical comparisons of Fourier and response spectra in Figs. 12 and 13 respectively, while Fig. 14 depicts comparison of response spectral variability with the regional GMPEs. For graphical comparison in Figs. 12 and 13, we have chosen August 17, 1999 Kocaeli earthquake M_W 7.6. This choice of earthquake will also allow reader to appreciate the consistency of the point source model in simulating ground motions from rather large ruptures. In addition to the use in synthesizing ground motions for low seismicity regions the model parameters such as $\Delta\sigma$, geometrical spreading, Q and κ_0 are also used to represent the source, path and site attributes of empirical GMPEs in their HTTA (Host-to-Target Adjustment) framework. To that end, as depicted in Fig. 13, a good comparison of the response spectra obtained

Table 4 Seismological parameters derived from different studies

	Region	$G(R)$	Q	κ_0 (s)	$\Delta\sigma$ (MPa)
Kurtulmus and Akyol (2013)	Western Turkey	Frequency dependent ranging from 0.84 to 1.52 at $R \leq 200$ km	$60f^{01.4}$ $Q(10) = 1507$		
Akinci et al. (2014)	Eastern Turkey	$G(R) = \begin{cases} R^{-1} & R<40\,\text{km} \\ R^{-0.3} & 40<R<200\,\text{km} \end{cases}$	$100f^{0.43}$ $(10) = 269$	0.03	4–20
Akinci et al. (2013)	Anatolia, Turkey	$G(R) = \begin{cases} R^{-1} & R\leq 20\,\text{km} \\ R^{-0.8} & 20\leq R\leq 40\,\text{km} \\ R^{-0.7} & 40\leq R\leq 100\,\text{km} \\ R^{-0.5} & R\geq 100\,\text{km} \end{cases}$	$180f^{0.55}$ $(10) = 639$	0.045	10
Askan et al. (2014)	Northwestern Turkey		2164 Soft soil	0.0455	
Hatzidimitrou (1995)	Northern Greece	$G(R) = R^{-1}$ $10 \leq R \leq 70$ km	$85f^{0.91}$ $Q(10) = 691$		
Margaris and Boore (1998)	Greece	$G(R) = R^{-1}$ $R \leq 50$ km	$88f^{0.1}$ $Q(10) = 700$	0.06	5.6
Polatidis et al. (2003)	Hellenic arc Greece	$G(R) = \begin{cases} R^{-1} & R\leq 100\,\text{km} \\ R^{-2} & R>100\,\text{km} \end{cases}$	$55f^{0.91}$ $Q(10) = 447$		
Malagnini et al. (2000)	Central Europe	$G(R) = \begin{cases} R^{-0.8} & R\leq 140\,\text{km} \\ R^{-1.5} & 140\leq R\leq 180\,\text{km} \\ R^{0} & 180\leq R\leq 220\,\text{km} \\ R^{-0.5} & R\geq 220\,\text{km} \end{cases}$	$400f^{0.42}$ $Q(10) = 1052$	0.05	3
Edwards and Fäh (2013a)	Europe and Middle East	R^{-1} $R < 100$ km	619–716	0.032–0.033	8.8
Malagnini and Herrmann (2000)	Umbria-Marche Italy	R^{-1} $R < 50$ km	$130f^{0.1}$ $Q(10) = 164$	0.04	20
Malagnini et al. (2002)	Northeastern Italy	Frequency and distance dependent at $R \leq 200$ km	$260f^{0.55}$ $Q(10) = 922$	0.045	60
Malagnini et al. (2011)	L'Aquila	$G(R) = \begin{cases} R^{-1.1} & R\leq 10\,\text{km} \\ R^{-1.} & 10\leq R\leq 30\,\text{km} \\ R^{-0.7} & R>30\,\text{km} \end{cases}$	$140f^{0.25}$ $Q(10) = 249$		

Table 4 continued

	Region	$G(R)$	Q	κ_0 (s)	$\Delta\sigma$ (MPa)
Pacor et al. (2016)	L'Aquila	$G(R) = \begin{cases} R^{-1.08} & R \le 10\,\text{km} \\ R^{-1.64} & 10 \le R \le 70\,\text{km} \\ R^{-0.64} & R > 70\,\text{km} \end{cases}$	$290f^{0.16}$ $Q(10) = 419$	0.012	0.1–25
This study	Europe and Mediterranean	$G(R) = \begin{cases} R^{-1.14} & R \le 70\,\text{km} \\ R^{-0.5} & 70 < R \le 225\,\text{km} \end{cases}$	$\begin{cases} 610 & R \le 40\,\text{km} \\ 1152 & R > 40\,\text{km} \end{cases}$	0.031	5.65
This study	Italy	$G(R) = \begin{cases} R^{-1.14} & R \le 70\,\text{km} \\ R^{-0.5} & 70 < R \le 225\,\text{km} \end{cases}$	601	0.026	
This study	Turkey	$G(R) = \begin{cases} R^{-1.14} & R \le 70\,\text{km} \\ R^{-0.5} & 70 < R \le 225\,\text{km} \end{cases}$	1462	0.046	
This study	Remaining (mainly Greece)	$G(R) = \begin{cases} R^{-1.14} & R \le 70\,\text{km} \\ R^{-0.5} & 70 < R \le 225\,\text{km} \end{cases}$	780	0.033	

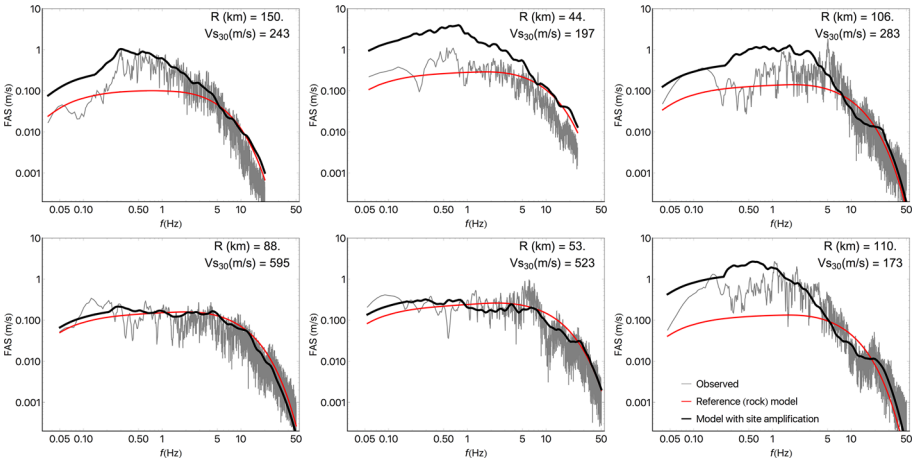

Fig. 12 Example of Fourier spectral fits to the observed recordings from M_W 7.6 Kocaeli earthquake (August 17, 1999). The model predictions (*heavy line*) are shown for inverted M_W 7.5, $\Delta\sigma$ = 9.1 MPa and station-specific κ_0 and amplifications

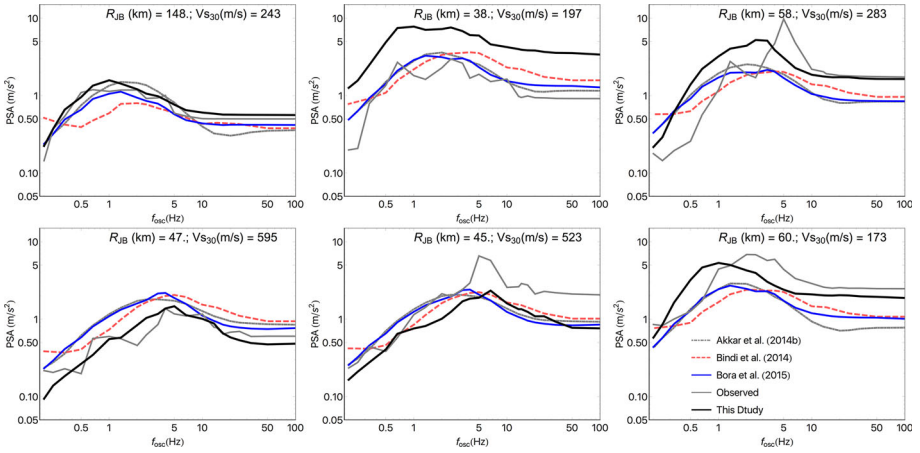

Fig. 13 Pseudo spectral acceleration (PSA) for Kocaeli records corresponding to the plots shown in Fig. 12. PSA from Akkar et al. (2014b), Bindi et al. (2014) and Bora et al. (2015) are also shown for comparison

from our stochastic model with the regional GMPEs of Akkar et al. (2014b), Bora et al. (2015) and Bindi et al. (2014) warrants the use of the present model in such exercises.

Figure 14 depicts comparison of response spectral variability obtained from the present stochastic model with the regional empirical models (Akkar et al. 2014b; Bindi et al. 2014; Bora et al. 2015). Response spectral residuals were obtained for an average $\Delta\sigma = 5.65$ MPa and site amplification curves for the stations recording at least four component-records, with measured Vs_{30} measurements along with the regional Q_0 and corresponding station-specific κ_0 values. The residuals were decomposed into between- and within-event components by performing a linear (intercept-only) mixed-effects

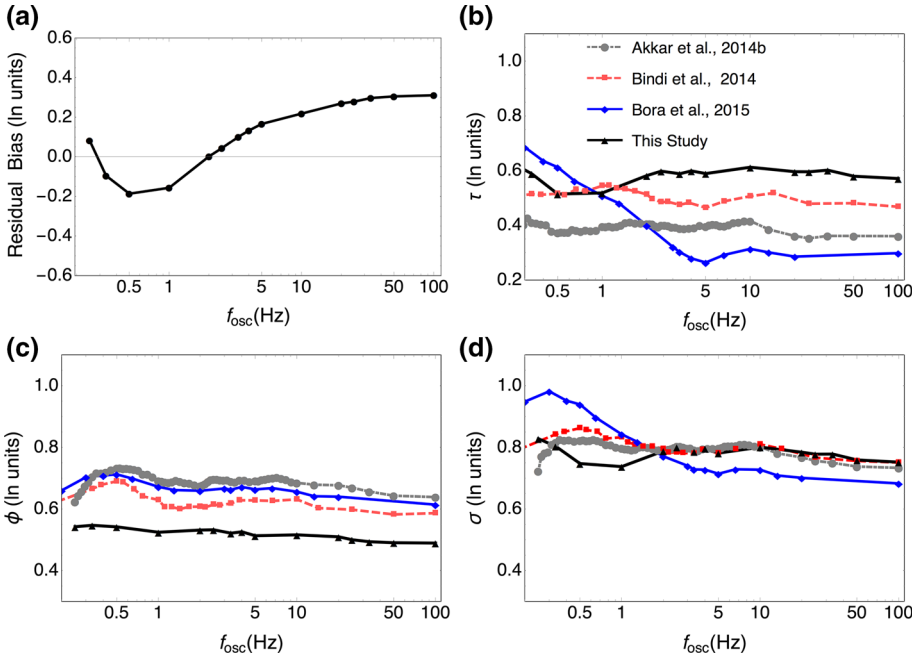

Fig. 14 Comparison of response spectral variability from the derived stochastic model (using median $\Delta\sigma = 5.65$ MPa, regional Q along with station-specific κ_0 and amplifications) with that from regional empirical models. **a** Residual bias, **b** between-event variability (τ), **c** within-event variability (Φ), **d** total variability (σ). The variability from Bora et al. (2015) corresponds to the curve (in their Fig. 17) that is obtained with event-specific $\Delta\sigma$ and station-specific κ_0

regression (*lme4* package, Bates et al. 2015) on the total residuals. Figure 14a depicts the mean residual bias at each oscillator frequency; Fig. 14b depicts between-event standard deviation (τ); Fig. 14c depicts within-event standard deviation (Φ) and Fig. 14d depicts the total standard deviation (σ). Significant reduction in within-event variability (Φ) is mainly due to capturing the between-station variability in terms of site amplification and κ_0 in the model itself. Also, capturing the regional variability in Q_0 has also led to further reduction in Φ.

9 Conclusions

This study was aimed at providing measurements of regional source, attenuation and site parameters for Europe and the Mediterranean region based upon a subset-dataset (Bora et al. 2015) of RESORCE-2012 database. Estimation of source, path and site parameters is based upon the far-field spectral representation of strong ground motion phases. In which, the source is represented by a Brune (1970) single corner frequency (f_c) model. The path effects are modeled using simple geometrical and inelastic attenuation models. The inelastic attenuation is parameterized in terms of a frequency-independent Q_0 model (Edwards et al. 2008; Campbell 2009; Edwards and Fäh 2013a). As detailed in Bora et al. (2015), to enable the validity of point source model, near distance records from moderate and large magnitude earthquakes have been discarded. In the first stage, we fit for source-

corner frequency f_c and attenuation operator t^* by fixing the M_0 to a value obtained from database M_W (Hanks and Kanamori 1979).

The inverted t^* values from the full dataset indicate a Q_0 model varying with distance that essentially captures depth-dependent Q structure (Edwards et al. 2008, 2011). However, a clear regional variation in inelastic attenuation (Q_0) is observed with a large value of Q_0, i.e., 1462 (smaller attenuation) for Turkey and smaller Q_0 (larger attenuation) of 601 for Italy. We also investigated κ_0 variability in terms of between-station and within-station (record-to-record) components indicating a large contribution in within-station variability through regional and depth variations of Q. Station-specific average Fourier site amplification factors were obtained with respect to a reference site with shear wave velocity (Vs) profile of California (Boore and Joyner 1997) anchored at Vs_{30} 620 m/s. The base (or hard-rock) model is described in terms of seismic moments obtained from database M_W, *a priori* geometrical spreading function and regional Q models along with the station κ_0. To cover a broader range of stations, site-class specific site amplification factors were also estimated.

In the second stage of inversion, the observed Fourier spectra were corrected for site-class specific amplification factor and subsequently further inverted to obtain the Brune's corner frequency f_c and M_0. The fitting procedure involves all the records from an event where the high frequency shape of each record was constrained by using the regional Q models along with the site-class κ_0. Despite having very few events with a large number of multiple recordings, the inverted M_W values were found broadly consistent with the database M_W. The estimated $\Delta\sigma$ from inverted f_c and M_0 did not exhibit dependence over magnitude. The database common $\Delta\sigma$ was estimated to be 5.75 and 5.65 MPa using inverted and database M_W respectively. The $\Delta\sigma$ values obtained in this study were observed

Table 5 Seismological parameters for Europe and Mediterranean stochastic model

Parameter	Parameter estimate
Source spectrum	Brune single corner f_c point source
Stress parameter $\Delta\sigma$	5.75 MPa with inverted M_W, Std. Dev. 0.43 in log units
	5.65 MPa with database M_W, Std. Dev. 0.33 in log units
Geometrical spreading	$R^{-1.14}$ for $R \leq 70$ km
	$R^{-0.5}$ for $R > 70$ km
Inelastic attenuation Q_0	610 for $R \leq 40$ km
	1152 for $R > 40$ km
	For Turkey: 1462; 68% confidence limits: 1333, 1620
	For Italy: 601; 68% confidence limits: 566, 640
Shear wave velocity β	3.5 km/s
Density ρ	2800 kg/m^3
Site attenuation κ_0 (s)	0.0308, standard error: 0.0024
	For Turkey: 0.0457, standard error: 0.002
	For Italy: 0.0261, standard error: 0.0015
Site amplification	Station and site-class specific from residual analysis
Reference rock site amplification	California generic rock anchored at Vs_{30} 620 m/s (Boore and Joyner 1997)

to be in good comparison with the previous studies involving earthquakes from the same region. Although, we did not observe a clear regional dependence of $\Delta\sigma$ mainly because of the limited dataset, the St. Die earthquake M_W 4.8 located at French–German border was found to be exhibiting a relatively high $\Delta\sigma$ of 32.3 MPa. We would like to mention here, what is already noted by Atkinson and Beresnev (1997), that the $\Delta\sigma$ values obtained in this way do not represent the actual drop in stress (before and after the earthquake) one would expect during an earthquake rupturing, but rather a measure of the proportion of radiated high-frequencies.

Finally, we note that the inversion of spectral parameters in Bora et al. (2015) was focused on a record-wise fitting of each spectrum to enable a consistent extrapolation beyond the filter high-pass and low frequencies. While, this study is aimed at discussing current challenges that are associated with stochastic modelling of ground motion, thus providing robust estimates of regional stochastic model parameters for Europe and Mediterranean region. Furthermore, the present study is believed to facilitate an updated reference stochastic model, presented in Table 5, for Europe and Mediterranean regions.

10 Data and resources

Data was taken from the RESORCE database (Akkar et al. 2014a). Figures were prepared using the program Mathematica except Fig. 1a was prepared using GMT (The Generic Mapping Tools). The linear mixed effects regression was performed using R-package *lme4* (Bates et al. 2015).

Acknowledgements This work was funded by the SIGMA Project. Dino Bindi and Olga Ktenidou are thanked for their useful discussions, comments and feedbacks. Solveig Strutzke is thanked for useful help in formatting the manuscript.

References

Abrahamson NA, Silva WJ, Kamai R (2014) Summary of the ASK14 ground motion relation for active crustal regions. Earthq Spectra 30:1025–1055

Aki K (1967) Scaling laws of seismic spectrum. J Geophys Res 72:1217–1231

Akinci A, D'Amico S, Malagnini L, Mercuri A (2013) Scaling earthquake ground motions in western Anatolia, Turkey. Phys Chem Earth 63:124–135

Akinci A, Malagnini L, Herrmann R, Kalafat D (2014) High-frequency attenuation in the Lake Van Region, Eastern Turkey. Bull Seismol Soc Am 104(3):1400–1409

Akkar S, Sandıkkaya MA, Şenyurt M, Azari Sisi A, Ay BÖ, Traversa P, Douglas J, Cotton F, Luzi L, Hernandez B, Godey S (2014a) Reference database for seismic ground-motion in Europe (RESORCE). Bull Earthq Eng 12(1):311–339

Akkar S, Sandikkaya MA, Bommer JJ (2014b) Empirical ground-motion models for point- and extended-source crustal earthquake scenarios in Europe and the Middle East. Bull Earthq Eng 12(1):359–387

Anderson JG (1991) A preliminary descriptive model for the distance dependence of the spectral decay parameter in Southern California. Bull Seismol Soc Am 81:2186–2193

Anderson JG, Hough SE (1984) A model for the shape of the fourier amplitude spectrum of acceleration at high frequencies. Bull Seismol Soc Am 74(5):1969–1993

Askan A, Sisman F, Pekcan O (2014) A regional near-surface high frequency spectral attenuation (kappa) model for northwestern Turkey. Soil Dyn Earthq Eng 65:113–125

Atkinson GM (2004) Empirical attenuation of ground-motion spectral amplitudes in Southeastern Canada and the Northeastern United States. Bull Seismol Soc Am 94(3):1079–1095

Atkinson GM, Beresnev I (1997) Don't call it stress drop. Seismol Res Lett 68(1):3–4

Atkinson GM, Boore DM (2011) Modifications to existing ground-motion prediction equations in light of new data. Bull Seismol Soc 101(3):1121–1135

Atkinson GM, Mereu RF (1992) The shape of ground motion attenuation curves in Southeastern Canada. Bull Seismol Soc Am 82(5):2014–2031
Atkinson GM, Morrison M (2009) Observations on regional variability in ground-motion amplitudes for small-to-moderate earthquakes in North America. Bull Seismol Soc Am 99:2393–2409
Baltay AS, Hanks TC (2014) Understanding the magnitude dependence of PGA and PGV in NGA-West 2 data. Bull Seismol Soc Am 104(6):2851–2865
Bates D, Maechler M, Bolker B, Walker S (2015) Fitting linear mixed-effects models using lme4. J Stat Softw 67:1–48
Bay F, Fäh D, Malagnini L, Giardini D (2003) Spectral shear-wave ground-motion scaling in Switzerland. Bull Seismol Soc 93(1):414–429
Bindi D, Massa M, Luzi L, Ameri G, Pacor F, Puglia R, Augliera P (2014) Pan-European ground-motion prediction equations for the average horizontal component of PGA, PGV, and 5%-damped PSA at spectral periods up to 3.0 s using the RESORCE dataset. Bull Earthq Eng 12(1):391–430
Boore DM (1983) Stochastic Simulation of high frequency ground motions based on seismological models of the radiated spectra. Bull Seismol Soc Am 73(6):1865–1894
Boore DM (2003) Simulation of ground motion using the stochastic method. Pure appl Geophys 160(3):635–676
Boore DM, Boatwright J (1984) Average body-wave radiation coefficients. Bull Seismol Soc Am 74(5):1615–1621
Boore DM, Joyner WB (1997) Site amplifications for generic rock sites. Bull Seismol Soc Am 87(2):327–341
Boore DM, Stewart JP, Seyhan E, Atkinson GM (2014) NGA-West2 equations for predicting PGA, PGV, and 5% damped PSA for shallow crustal earthquakes. Earthq Spectra 30(3):1057–1085
Bora SS, Scherbaum F, Kuehn N, Stafford P (2014) Fourier spectral- and duration models for the generation of response spectra adjustable to different source-, propagation-, and site conditions. Bull Earthq Eng 12(1):467–493
Bora SS, Scherbaum F, Kuehn N, Stafford P, Edwards B (2015) Development of a response spectral ground-motion prediction equation (GMPE) for seismic-hazard analysis from empirical fourier spectral and duration models. Bull Seismol Soc Am 105(4):2192–2218
Brune JN (1970) Tectonic stress and the spectra of seismic shear waves from earthquakes. J Geophys Res 75(26):4997–5009
Brune JN (1971) Correction. J Geophys Res 76(20):5002
Campbell KW (2003) Prediction of strong ground motion using the hybrid empirical method and its use in the development of ground-motion (Attenuation) relations in Eastern North America. Bull Seismol Soc Am 93(3):1012–1033
Campbell KW (2009) Estimates of shear-wave q and kappa(0) for un- consolidated and semi-consolidated sediments in eastern North America. Bull Seismol Soc Am 99:2365–2392
Campillo M, Bouchon M, Massinon B (1984) Theoretical study of the excitation, spectral characteristics, and geometrical attenuation of regional seismic phases. Bull Seismol Soc 74(1):79–90
Chandler AM, Lam NT, Sang HH (2006) Near-surface attenuation modelling based on rock shear-wave velocity profile. Soil Dyn Earthq Eng 26:1004–1014
Chen SZ, Atkinson GM (2002) Global comparisons of earthquake source spectra. Bull Seismol Soc Am 92(3):885–895
Cotton F, Archuleta R, Causse M (2013) What is sigma of the stress drop? Seismol Res Lett 84(1):42–48
Derras B, Bard PY, Cotton F (2014) Towards fully data driven ground-motion prediction models for Europe. Bull Earthq Eng 12(1):495–516
Douglas J, Jousset P (2011) Modeling the difference in ground-motion magnitude scaling in small and large earthquakes. Seismol Res Lett 82(4):504–508
Douglas J, Gehl P, Bonilla LF, Gelis C (2010) A kappa model for mainland France. Pure appl Geophys 167:1303–1315
Drouet S, Chevrot S, Cotton F, Souriau A (2008) Simultaneous inversion of source spectra, attenuation parameters, and site responses: application to the data of the french accelerometric network. Bull Seismol Soc Am 98(1):198–219
Drouet S, Cotton F, Gueguen P (2010) nu(S30), kappa, regional attenuation and Mw from accelerograms: application to magnitude 3–5 French earthquakes. Geophys J Internat 182(2):880–898
Edwards B, Fäh D (2013a) Measurements of stress parameter and site attenuation from recordings of moderate to large earthquakes in Europe and the Middle East. Geophys J Internat 194(2):1190–1202
Edwards B, Fäh D (2013b) A stochastic ground-motion model for Switzerland. Bull Seismol Soc Am 103(1):78–98

Edwards B, Rietbrock A (2009) A comparative study on attenuation and source-scaling relations in the Kanto, Tokai, and Chubu regions of Japan, using data from Hi-net and kik-net. Bull Seismol Soc Am 99:2435–2460

Edwards B, Rietbrock A, Bommer JJ, Baptie B (2008) The Acquisition of source, path, and site effects from microearthquake recordings using Q tomography: application to the United Kingdom. Bull Seismol Soc Am 98(4):1915–1935

Edwards B, Fäh D, Giardini D (2011) Attenuation of seismic shear wave energy in Switzerland. Geophys J Internat 185(2):967–984

Edwards B, Michel C, Poggi V, Fäh D (2013) Determination of site amplification from regional seismicity: application to the Swiss National Seismic Networks. Seismol Res Lett 84(4):611–621

Edwards B, Ktenidou OJ, Cotton F, Abrahamson N, Van Houtte C, Fäh D (2015) Epistemic uncertainty and limitations of the κ0 model for near-surface attenuation at hard rock sites. Geophys J Internat 202(3):1627–1645

Edwards B, Cauzzi C, Danciu L, Fäh D (2016) Region-specific assessment, adjustment and weighting of ground motion prediction models: application to the 2015 Swiss Seismic Hazard Maps. Bull Seismol Soc Am 106(4):1840–1857

Eshelby JD (1957) The determination of the elastic field of an ellipsoidal inclusion, and related problems. The determination of the elastic field of an ellipsoidal inclusion, and related problems. Proc R Soc Lond Ser A Math Phys Sci 241:376–396

Goertz-Allmann BP, Edwards B (2014) Constraints on crustal attenuation and three-dimensional spatial distribution of stress drop in Switzerland. Geophys J Int 196:493–509

Hanks TC (1979) B values and ω^{-y} seismic source models: implications for tectonic stress variations along active crustal fault zones and the estimation of high-frequency strong ground motion. J Geophys Res 84:2235–2242

Hanks TC, Kanamori H (1979) A moment magnitude scale. J Geophys Res B Solid Earth 84:2348–2350

Hanks TC, McGuire RK (1981) The character of high-frequency strong ground motion. Bull Seismol Soc Am 71(6):2071–2095

Hatzidimitrou PM (1995) S-wave attenuation in the crust in northern Greece. Bull Seismol Soc Am 85(5):1381–1387

Hermkes M, Kuehn N, Riggelsen C (2014) Simultaneous quantification of epistemic and aleatory uncertainty in GMPEs using Gaussian process regression. Bull Earthq Eng 12:449–466

Hough SE, Anderson JG, Brune J, Vernon F, Berger J, Fletcher J, Haar L, Hanks L, Baker L (1988) Attenuation near Anza,California. Bull Seismol Soc Am 78(2):672–691

Joyner WB, Warrick RE, Fumal TE (1981) The effect of quaternary alluvium on strong ground motion in the Coyote Lake, California, earthquake of 1979. Bull Seismol Soc Am 71(4):1333–1349

Kilb D, Glenn B, Anderson JG, Brune J, Zhigang P, Vernon F (2012) A comparison of spectral parameter kappa from small and moderate earthquakes using Southern California ANZA seismic network data. Bull Seismol Soc Am 102(1):284–300

Konno K, Ohmachi T (1998) Ground-motion characteristics estimated from spectral ratio between horizontal and vertical components of microtremor. Bull Seismol Soc America 88(1):228–241

Kotha SR, Bindi D, Cotton F (2016) Partially non-ergodic region specific GMPE for Europe and Middle-East. Bull Earthq Eng 14(4):1245–1263

Ktenidou O-J, Cotton F, Abrahamson NA, Anderson JG (2014) Taxonomy of kappa: a review of definitions and estimation approaches targeted to applications. Seismol Res Lett 85(1):135–146

Ktenidou O-J, Abrahamson NA, Drouet S, Cotton F (2015) Understanding the physics of kappa (κ): insights from a downhole array. Geophys J Int 203:678–691

Kuehn N, Scherbaum F (2016) A partially non-ergodic ground-motion prediction equation for Europe and the Middle East. Bull Earthq Eng 14(10):2629–2641

Kurtulmus TÖ, Akyol N (2013) Crustal attenuation characteristics in western Turkey. Geophys J Int 195:1384–1395

Malagnini L, Herrmann RB (2000) Ground-motion scaling in the region of the 1997 Umbria-Marche Earthquake (Italy). Bull Seismol Soc America 90(4):1041–1051

Malagnini L, Herrmann RB, Koch K (2000) Regional ground-motion scaling in Central Europe. Bull Seismol Soc America 90(4):1052–1061

Malagnini L, Akinci A, Herrmann RB, Pino NA, Scognamiglio L (2002) Characteristics of the ground motion in Northeastern Italy. Bull Seismol Soc America 92(6):2186–2204

Malagnini L, Scognamiglio L, Mercuri A, Akinci A, Mayeda K (2008) Strong evidence for non-similar earthquake source scaling in central Italy. Geophys Res Lett 35:L17303

Malagnini L, Akinci A, Mayeda K, Munafo I, Herrmann RB, Mercuri A (2011) Characterization of earthquake-induced ground motion from the L'Aquila seismic sequence of 2009, Italy. Geophys J Int 184:325–337

Margaris BN, Boore D (1998) Determination of $\Delta\sigma$ and $\kappa 0$ from response spectra of large earthquakes in Greece. Bull Seismol Soc Am 88(1):170–182

McGuire RK, Hanks TC (1980) RMS acceleration and spectral amplitudes of strong ground-motion during the San Fernando, California earthquake. Bull Seismol Soc Am 70(5):1907–1919

Molkenthin C, Scherbaum F, Griewank A, Kuehn N, Stafford PJ (2014) A Study of the sensitivity of response spectral amplitudes on seismological parameters using algorithmic differentiation. Bull Seismol Soc Am 104(5):2240–2252

Morozov IB (2008) Geometrical attenuation, frequency dependence of Q, and the absorption band problem. Geophys J Int 175:239–252

Morozov IB (2009) Thirty years of confusion around "scattering Q"? Seismol Res Lett 80:5–7

Pacor F, Spallarossa D, Oth A, Luzi L, Puglia R, Cantore L, Mercuri A, D'Amico M, Bindi D (2016) Spectral models for ground motion prediction in the L'Aquila region (central Italy): evidence for stress-drop dependence on magnitude and depth. Geophys J Int 204:697–718

Parolai S, Bindi D (2004) Influence of soil-layer properties on k evaluation. Bull Seismol Soc Am 94(1):349–356

Poggi V, Edwards B, Fäh D (2011) Derivation of a reference shear-wave velocity model from empirical site amplification. Bull Seismol Soc Am 101(1):258–274

Polatidis A, Kiratzi A, Hatzidimitriou PM, Margaris B (2003) Attenuation of shear-waves in the back-arc region of the Hellenic arc for frequencies from 0.6 to 16 Hz. Tectonophysics 367:29–40

Scherbaum F, Schmedes J, Cotton F (2004) On the conversion of source-to-site distance measures for extended earthquake source models. Bull Seismol Soc Am 94(3):1053–1069

Singh SK, Apsel J, Fried J, Brune JN (1982) Spectral attenuation of SH waves along the imperial fault. Bull Seismol Soc Am 72(6):2003–2016

Van Houtte C, Drouet S, Cotton F (2011) Analysis of the origins of kappa (Kappa) to compute hard rock to rock adjustment factors for GMPEs. Bull Seismol Soc Am 101(6):2926–2941

Yenier E, Atkinson GM (2015a) An equivalent point-source modeling of moderate-to-large magnitude earthquakes and associated ground-motion saturation effects. Bull Seismol Soc Am 105(3):1435–1455

Yenier E, Atkinson GM (2015b) Regionally adjustable generic ground-motion prediction equation based on equivalent point-source simulations: application to central and eastern North America. Bull Seismol Soc Am 105(4):1989–2009